2021

Finite Different Time-Domain Simulation of Terahertz Waves Propagation Through Unmagnetized Plasma

Aditha Srikantha Senarath
Wright State University

FINITE DIFFERENT TIME DOMAIN SIMULATION OF TERAHERTZ WAVES PROPAGATION THROUGH UNMAGNETIZED PLASMA

A thesis submitted in partial fulfilment of the
requirements for the degree of
Master of Science

By

ADITHA SRIKANTHA SENARATH
B.Sc., The University of Peradeniya, Srilanka 2016

2021
Wright State University

WRIGHT STATE UNIVERSITY

GRADUATE SCHOOL

Aug 6, 2021

I HEREBY RECOMMEND THAT THE THESIS PREPARED UNDER MY SUPERVISION BY Aditha Srikantha Senarath ENTITLED Finite Different Time Domain Simulation of Terahertz Waves Propagation Through Unmagnetized Plasma BE ACCEPTED IN PARTIAL FULFILLMENT OF THE REQUIREMENTS FOR THE DEGREE OF Master of Science

_____

Jason A. Deibel, Ph. D.
Thesis Director

_____

Jason A. Deibel, Ph. D.
Chair, Department of Physics

Committee on
Final Examination

_____
Jason A. Deibel, Ph. D.

_____
Sarah F. Tebbens, Ph. D.

_____
Amit R. Sharma, Ph. D.

_____
Barry Milligan, Ph.D.
Vice Provost for Academic Affairs
Dean of the Graduate School

ABSTRACT

Senarath, Aditha Srikantha. M.S. Department of Physics, Wright State University, 2021. Finite Different Time Domain Simulation of Terahertz Waves Propagation Through Unmagnetized Plasma

In order to support ongoing terahertz time-domain spectroscopic experiments involving plasma characterization, it is beneficial to simulate the interaction of THz pulses with varying plasma configurations. In this approach, a 1-D Finite Difference Time Domain (FDTD) model was constructed to simulate the interaction of terahertz radiation with a plasma medium. In order to incorporate the plasma properties into the simulation, a Z-transformation was applied. This model is capable of simulating the following properties of plasmas including electron density, collision frequency, and the interaction length of the plasma medium. The simulated model was characterized using terahertz time-domain spectroscopy. The effects of electron density, collision frequency, and the interaction length of the plasma medium on the amplitude and phase of the terahertz pulse were studied and calculated values of electron density were compared with the values used in simulation.

TABLE OF CONTENT

LIST OF FIGURES

LIST OF TABLES

1. INTRODUCTION

1.1 Overview of Plasma

There are four states of matter but three of them are more common and well understood. Those are the solid, liquid, and gas states. The fourth state is plasma, which is an area of active and increasing research activity. Increasing the temperature of solids and liquids transforms them into liquids and gases, respectively. Similar to those phase changes, if the temperature of a gas is sufficiently increased, it becomes a plasma.

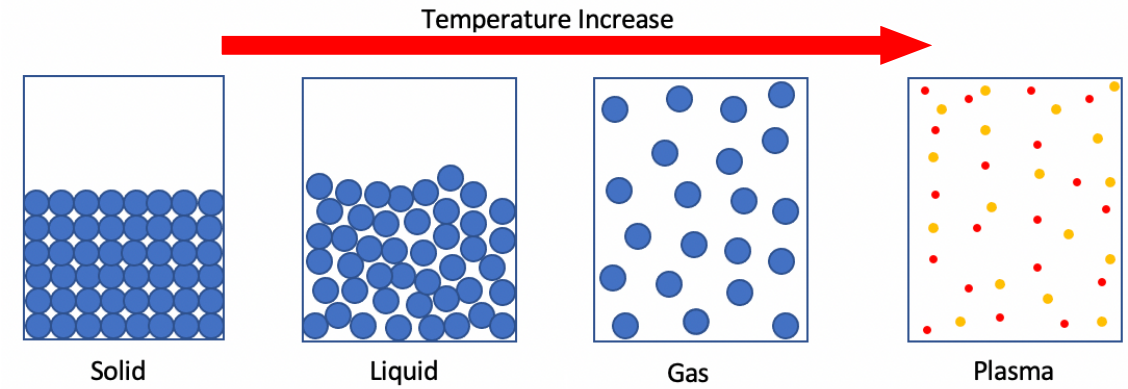

Figure 1.1: Relative atomic arrangement of four states of matter.

From the molecular point of view, in solids, molecules are closely arranged and don't have much freedom to move. In liquids, the molecules are not so closely arranged and

can flow around each other. In gases, molecules are very loosely bound and have a very high amount of kinetic energy. Finally, plasmas are somewhat similar to the gaseous state, but there are highly charged particles instead of molecules in the other three states [1].

For a plasma medium, the plasma frequency is defined as

$$\omega_p = \sqrt{\frac{n_e e^2}{\varepsilon_0 m}} \tag{1.1}$$

where: n_e is the free electron density, e is the charge of an electron, m is the mass of an electron and ε_0 is the permittivity of free space. This frequency is called the fast electron plasma frequency. The plasma frequency is a measure of how fast the plasma medium responds to an external disturbance such as an incident electromagnetic wave or particle beam. The relationship between the plasma response time (t_D) and the plasma frequency is given in Eqn. 1.2,

$$t_D = \frac{2\pi}{\omega_p} \tag{1.2}$$

If the plasma response time is less than the period of external disturbance, that disturbance cannot go inside or through the plasma. For example, consider that the disturbance is an electromagnetic wave with wavelength λ such that the period of the electromagnetic wave is denoted

$$t = \frac{1}{f} = \frac{\lambda}{c} \tag{1.3}$$

If the ration of these two times is taken,

$$\frac{t}{t_D} = \frac{\lambda \omega_p}{2\pi c} \tag{1.4}$$

When a plasma is transparent to an incident electromagnetic wave, the above ratio will be greater than 1 and when the plasma is opaque, the ratio will be less than 1. Plasma transparency occurs for electromagnetic waves with a wavelength less than $\frac{2\pi c}{\omega_p}$ and opacity for electromagnetic waves with wavelengths greater than $\frac{2\pi c}{\omega_p}$. At the plasma frequency, this ratio is equal to 1. That means electrons in the plasma medium oscillate with the frequency equal to the plasma frequency. At that point all most all of the energy in the electromagnetic radiation absorbed by the plasma medium. If the frequency of the electromagnetic wave is higher than the plasma frequency but near to the plasma frequency, the plasma medium absorbs some amount of the radiation and transmit others [2].

1.1.1. Electromagnetic Waves in Plasma.

The oscillating electric field in the electromagnetic wave, oscillate the electrons in the plasma medium. That oscillation is damped by the electron-electron collisions and electron-ion collisions. Average number of such collisions in a unit time is defined as the collision frequency.

The 1-D equation of motion for a cold isotropic plasma with collision frequency ν_c is defined as,

$$\frac{d^2x(t)}{dt^2} + \nu_c \frac{dx(t)}{dt} = -\frac{e}{m} E(t) \tag{1.5}$$

where $x(t)$ is the displacement, e is the charge of an electron, m is the mass of an electron, ν_c is the collision frequency, and $E(t)$ is the time-dependent electric field, with the time-varying electric field defined as,

$$E(t) = E_0(\omega)e^{i\omega t} \quad 1.6$$

Assume the solution of Equation 1.5 is in the form of Equation 1,7,

$$x(t) = \chi_0(\omega)e^{i\omega t} \quad 1.7$$

where $\chi_0(\omega)$ is the maximum displacement of the electron with frequency ω (complex amplitude)

After substituting Equations 1.6 and 1.7 into Equation 1.5 and solving for the complex amplitude ($\chi_0(\omega)$),

$$\chi_0(\omega) = \frac{e}{m}\frac{E_0(\omega)}{(\omega^2 - i\omega\nu_c)} \quad 1.8$$

The polarization is defined as the dipole moment per unit volume. Therefore, polarization can be expressed as,

$$P(\omega) = -en_e\chi_0(\omega) \quad 1.9$$

where $n_e$is the number of free electrons in a unit volume (electron density) and e is the charge of an electron.

$$P(\omega) = -\frac{n_e e^2}{m}\frac{E_0(\omega)}{(\omega^2 - i\omega\nu_c)} \quad 1.10$$

The complex electric susceptibility can then be defined as,

$$\mathbb{X} = \frac{P(\omega)}{\varepsilon_0 E_0(\omega)} \tag{1.11a}$$

Using Equations 1.10 and 1.11a

$$\mathbb{X} = -\frac{n_e e^2}{\varepsilon_0 m}\frac{E_0(\omega)}{(\omega^2 - i\omega\nu_c)} \tag{1.11b}$$

$$\mathbb{X} = -\frac{\omega_p^2}{(\omega^2 - i\omega\nu_c)} \tag{1.11c}$$

where: $\omega_p = \sqrt{\frac{n_e e^2}{\varepsilon_0 m}}$, the complex permittivity is then defined as

$$\varepsilon(\omega) = \varepsilon_0\big(1 + \mathbb{X}(\omega)\big) \tag{1.12a}$$

$$\frac{\varepsilon(\omega)}{\varepsilon_0} = 1 - \frac{\omega_p^2}{(\omega^2 - i\omega\nu_c)} \tag{1.12b}$$

$\frac{\varepsilon(\omega)}{\varepsilon_0}$ is called the Lorentz dielectric constant (ε_r)

$$\varepsilon_r = 1 - \frac{\omega_p^2}{(\omega^2 - i\omega\nu_c)} \tag{1.13}$$

[3]

1.2 THz Radiation and Spectroscopy.

Terahertz (THz) radiation belongs to the part of the electromagnetic spectrum and spans the frequency range from 0.3 to 10 THz. It is often referred to as submillimeter radiation. The corresponding wavelength range of THz radiation is 0.1 mm to 1 mm and corresponds to 1.2 to 12.4 meV in terms of photon energy. The equivalent temperature

range is roughly 14 to 140 K. This energy is in the range of molecular interaction, not atomic interaction. Therefore, THz radiation is very important for the study of low-frequency modes in molecular crystals. THz radiation is ideal for measuring charge carriers in semiconductors. [4]

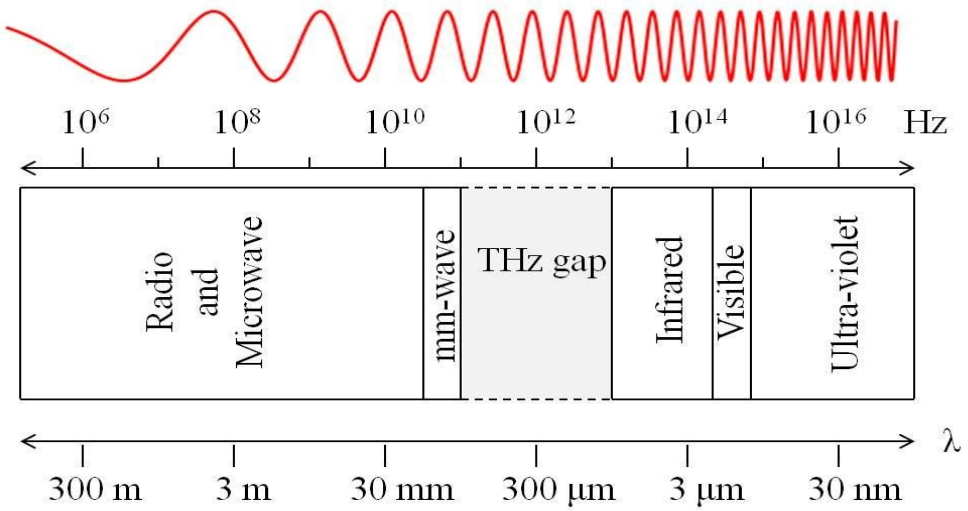

Figure 1.2: Electromagnetic Spectrum [5].

Any object within the 14 to 140 K temperature range emits THz radiation via black-body radiation. There are other artificial sources of THz radiation such as Mercury lamps, free electron lasers, quantum cascade lasers, diode systems, and photoconductive switches [6].

There are a number of applications of terahertz radiation in the fields of chemistry, materials sciences, engineering, and medicine such as THz imaging [7], molecular spectroscopy, and THz communication [8], because THz waves are safe and transmit through a variety of materials except for metals. Most of these applications still reside at the research level.

1.2.1 THz Spectroscopy.

THz Spectroscopy is a very active and fast-growing field of research in chemistry, material science, engineering, and medicine. THz spectroscopy is a powerful technique for material characterization and process control. One of the earliest THz Spectroscopy systems was based on the photoconductive switch and is still used for measurements around the frequency range of 1 THz. In the last few years, THz spectroscopy has developed a lot and the newer setups are often based on optical rectification and electro-optic sampling. These systems often provide increased bandwidth spanning 0.1 to 4 THz [6]. This spectroscopic technique is used to characterize a wide range of materials such as ceramics, semiconductors, environmental pollutants, chemical mixtures, and gases [9]. THz waves have been utilized in plasma diagnostics. The main advantage of using THz spectroscopy to characterize the plasma is that it provides the plasma properties directly through amplitude and phase information [3,10].

The magnitude of the photon energy associated with THz frequency radiation correlates to the energy levels associated with rotational transitions, low-frequency bond vibrations, crystalline phonon vibrations, hydrogen bond stretches, and torsion vibrations in materials. Both the generation and detection of THz pulses in THz-TDS is done in the time-domain. A Fourier transform of the time-dependent electric field yields both the frequency-dependent amplitude and phase. This is advantageous as it allows the technique to determine the refractive index and absorption coefficient of the material which can also lead to the determination of the materials' complex permittivity [8].

1.2.2 Terahertz Time-Domain Spectroscopy (THz-TDS)

This method was developed in the late 1980s and early 1990s. This method has found wide use for the spectroscopic and imaging-based characterization of many types of materials. Terahertz Time-Domain Spectroscopy (THz-TDS) has been used to determine plasma properties such as electron density, collision frequency, and plasma frequency. It is important to consider how plasma mediums interact with THz light and how certain plasma properties manipulate light.

As with other frequencies of electromagnetic waves, the electric field of THz radiation oscillates the charged particles in the interaction medium. These oscillating charged particles induce an electric field that interacts with the incident THz electric field. As a result of this interaction, the wavelength, amplitude, and phase of the THz radiation will be changed. Any consideration of the magnetic field can be neglected because the magnetic field amplitude value is negligible [4].

1.2.3 Index of refraction

The wavelength of a wave in a medium described by an index of refraction is

$$\lambda_m = \frac{\lambda_0}{n} \tag{1.14}$$

where λ_m is the wavelength in the medium, λ_0 is the vacuum wavelength of the incident wave, and n is the refractive index of the medium.

The amplitude of the incident wave and amplitude of the wave inside the medium is related to the absorption coefficient

$$A_f = A_0 exp\left(\frac{-\alpha}{2} L\right) \tag{1.15}$$

where A_f is amplitude inside the medium, A_0 is the amplitude of the incident wave, α is absorption coefficient and L is the length of the medium.

The amplitude of an electromagnetic wave after traveling a distance, d, through a medium can be written as

$$E(\omega) = E_0(\omega) exp\left(i\frac{\omega}{c}nd\right) \quad 1.16$$

where $E(\omega)$ is the amplitude of the electric field after traveling through the medium, $E_0(\omega)$ is the amplitude of the electric field before traveling through the medium, ω is the angular frequency of the electromagnetic wave, c is the speed of light in vacuum, n is the frequency-dependent refractive index of the medium and d is the thickness of the medium.

If the electromagnetic wave is traveling through the vacuum (n=1), the above equation becomes

$$E_{ref}(\omega) = E_0(\omega) exp\left(i\frac{\omega}{c}d\right) \quad 1.17$$

If a wave is traveling through a sample with refractive index n,

$$E_{sam}(\omega) = E_0(\omega) exp\left(i\frac{\omega}{c}nd\right) \quad 1.18$$

The ratio of these two electric fields is

$$\frac{E_{sam}(\omega)}{E_{ref}(\omega)} = exp\left(i\frac{\omega}{c}d(n-1)\right) \quad 1.19$$

The phase difference between the two waves is

$$|\Delta\emptyset| = \left|\emptyset_{sam} - \emptyset_{ref}\right| = \frac{\omega}{c}d(n-1) \quad 1.20$$

The frequency-dependent refractive index of the sample medium is derived from both waves as

$$n = 1 + \frac{c}{\omega d}|\Delta\emptyset| \tag{1.21}$$

[4,11]

1.2.4 Electron density

After separating the real and imaginary parts of Equation 1.13,

$$\varepsilon_r = 1 - \frac{\omega_p^2}{(\omega^2 - \nu_c^2)} + i\left(\frac{\omega_p^2 \nu_c}{\omega(\omega^2 + \nu_c^2)}\right) \tag{1.22}$$

One can write the complex refractive index using the relative permittivity,

$$n = \sqrt{\varepsilon_r} = \sqrt{1 - \frac{\omega_p^2}{(\omega^2 - \nu_c^2)} + i\left(\frac{\omega_p^2 \nu_c}{\omega(\omega^2 + \nu_c^2)}\right)} \tag{1.23}$$

After separating the real and imaginary parts of Equation 1.23,

$$n \tag{1.24}$$

$$= \sqrt{\frac{1}{2}\left(1 - \frac{\omega_p^2}{(\omega^2 + \nu_c^2)}\right) + \frac{1}{2}\sqrt{\left(1 - \frac{\omega_p^2}{(\omega^2 + \nu_c^2)}\right)^2 + \left(\frac{\omega_p^2 \nu_c}{\omega(\omega^2 + \nu_c^2)}\right)^2}}$$

$$+ i\sqrt{-\frac{1}{2}\left(1 - \frac{\omega_p^2}{(\omega^2 + \nu_c^2)}\right) + \frac{1}{2}\sqrt{\left(1 - \frac{\omega_p^2}{(\omega^2 + \nu_c^2)}\right)^2 + \left(\frac{\omega_p^2 \nu_c}{\omega(\omega^2 + \nu_c^2)}\right)^2}}$$

Substituting from Equation 1.24 into Equation 1.21

$$|\Delta\emptyset| = \frac{\omega L}{c}\left(\sqrt{\frac{1}{2}\left(1-\frac{\omega_p^2}{(\omega^2+\nu_c^2)}\right)+\frac{1}{2}\sqrt{\left(1-\frac{\omega_p^2}{(\omega^2+\nu_c^2)}\right)^2+\left(\frac{\omega_p^2\nu_c}{\omega(\omega^2+\nu_c^2)}\right)^2}-1}\right) \quad 1.25$$

Assuming, ω_p, ν_c << ω and using a Taylor series expansion.

$$|\Delta\emptyset| = \frac{\omega_p^2 L}{2c\omega} \quad 1.26$$

After substituting $\omega_p \ \ as \ \sqrt{\frac{n_e e^2}{\varepsilon_0 m}}$, the electron density ($n_e$) can be written as,

$$n_e = \frac{2c\omega\varepsilon_0 m_e|\Delta\emptyset|}{e^2 L} \quad 1.27$$

[10-12]

1.3 Motivation

Theoretical and experimental research were the main drivers of scientific research for several centuries. However, in the mid-20th century, a new tool, computers significantly altered both theoretical and experimental work. One aspect of this has been the development of computer simulations as they have played an important role in the development of many areas in science and engineering. The large increases in computational processing power over the last few decades have greatly advanced the scope and utility of computer simulation-driven research.

Simulation research plays an important role in the field of materials science these days. It is a useful tool for finding new materials and understanding material

phenomena. Computer simulation is a low-cost, safe and fast analysis tool. In material characterization, it is common to simulate the mathematical model in order to predict the properties and behaviors of the materials such as ceramics, semiconductors. Several simulation tools exist for computer simulations such as the finite-difference time-domain (FDTD), finite-element-method (FEM), density functional theory (DFT) and transmission-line-matrix (TLM) method [14].

As previously mentioned, the plasma state of matter is not as well understood as the other states of matter. There are lots of researchers doing experimental characterizations of plasma with different radiation in the last few decades. [3] Characterization is required in order to understand the properties of any materials and different wavelength ranges can be utilized to identify different properties of materials. The characterization of plasmas is necessary to better understand the physics of the plasma. Microwave and laser techniques are well-established tools for plasma characterization. There are several disadvantages of those methods. For example, the microwave method is accurate for low electron density plasmas and laser techniques are accurate for high electron density plasmas. These techniques require multiple sources in order to cover a wide range of electromagnetic frequencies. The THz-TDS method is a powerful technique to characterize plasma with a wide range of electron densities [13].

Since the plasma state is not a common state on the earth and it requires an advanced setup to achieve a plasma, it is very common and useful to use computer simulation to study plasma. Using those simulations, researchers can predict how THz

light can interact with plasma and solidify the theoretical understanding of experimental work. It is a very useful tool to develop and verify THz characterization techniques that can work with plasma.

1.4 Proposed Research

The purpose of this research was to develop a computer model that simulates the interaction of a plasma medium with incident THz radiation. The model could be used such that the plasma properties can be manipulated to study the effect of interacting THz light. This presentation of thesis research is organized as follows. First, the theoretical background is established by deriving the update equations for electric field and magnetic field inside the free space and plasma medium using FDTD method. This is followed by an analysis of THz pulse transmission through plasma using THz-TDS. The e interaction of THz radiation with plasma medium is discussed along with the effects of plasma properties onchanges to the amplitude and phase of THz pulse. The electron density and refractive index of plasma are calculated studying the change of phase in the interacting THz pulse. Finally, the calculated electron density values are compared with the value used in the computational model.

2. PREVIOUS WORK

The Finite Difference Time Domain (FDTD) method is one of the most famous and utilized methods for simulating electromagnetic phenomena and devices such as wave propagation, electromagnetic scattering, biocompatibility issues, and lumped devices [25]. This chapter describes previously reported FDTD simulation work and highlights experimental Terahertz Time-Domain characterization results.

2.1 FDTD simulations.

M. Wang et al. developed an FDTD simulation of terahertz wave propagation through a dusty plasma. FDTD simulations were coupled with Auxiliary Differential Equations (ADE) to study wave propagation in dusty plasmas which are best described as the plasma state with neutral particles usually in the micrometer and nanometer size range. Their model was used to examine the effect of the thickness, collision frequency, airborne particle density, and charge relaxation rate of airborne particles on the propagation of terahertz light. This included determining the variation of transmission coefficient, Reflection coefficient and absorption coefficient with different thicknesses of plasma medium. These simulation results indicated that the absorption coefficient increase with electron density, airborne particle density, thickness, and effective collision frequency, while it is insensitive to the charge relaxation rate [15].

P. J. Ford et al. developed an FDTD algorithm that calculated several radio frequency (RF) breakdown parameters including delay time and the breakdown electric field. The breakdown electric field is the electric field strength that shows a sharp drop of transmitted electric power. The delay time is the time taken to begin that sharp drop of transmitted electric power. The simulation used a Z-Transform to incorporate the complex frequency-dependent permittivity of plasma. Their results showed that the attenuation of the transmitted wave was proportional to the integral of the electron density, not the peak electron density. In the end, they emphasized some limitations of the 1D - FDTD method. The main drawback is how the model must assume average particle densities and energies. The simulations would have more utility of they were extended to 3D to model experimental geometries [26].

D. N. Smithe published work describing a FDTD simulation of fusion plasmas at radiofrequency. In a fusion plasma, the plasma state is maintained using a combination of internal and external heating by induction, radiation, or neutral particle injection. Their model is based on a cold plasma (plasma which is not in thermal equilibrium that means the electron and heavy particles are not at the same temperature) dielectric constant, and it is designed to provide a more accurate plasma description [27].

M. Liu et al, studied the attenuation of waves in a thin plasma layer using FDTD simulation. They have investigated the effect of plasma thickness, plasma density distribution function, collision frequency, and frequency of the incident light on the attenuation of electromagnetic waves. They considered two different plasma density

functions (hyperbolic tangent distribution and exponential distribution) instead of considering a homogeneous plasma density. Their numerical results suggested that phase shifts were determined by the plasma distribution, and that the attenuation of the wave depend on its frequency, plasma thickness, plasma density distribution, and collision frequency. The work further indicated that a large frequency range of microwaves can be absorbed if the thickness of the plasma layer is larger than 20 mm. The results showed that the attenuation of the wave was higher for the hyperbolic tangent distribution than exponential distribution [28].

2.2 Terahertz Time-Domain Spectroscopy (THz-TDS).

B. H. Kolner et al. presented a new plasma diagnostic system based on Terahertz Time-Domain Spectroscopy (THz-TDS). In their work, they simulated the propagation of a THz pulse through a plasma as function of varying electron densities and collision frequencies. They studied the varying of the shape of the transmitted THz pulse with different electron densities and collision frequencies. This work included a theoretical study that changed the complex refractive index of plasma with the pulse frequency and electron density. This report included a large body of experimental terahertz spectroscopic measurements of plasmas for comparison. Initially, the electron density was predicted using optical fluorescence images. In this work, they were able to record electron density and collision rates over ranges of $4x10^{11}$ cm^{-3} to $4.5x10^{13}$ cm^{-3} and $4.5x10^{10}$ s^{-1} to $8x10^{11}$ s^{-1}, respectively. They expected this new method to have applications in laser-plasma interaction and fusion turbulence studies [3].

B. H. Kolner et al. used THz characterization to study the time evolution of electron density and collision frequency of an Ar plasma. They studied a variety of electron densities and collision frequencies as a function of time delay between the ionizing current pulse into the plasma and THz probe pulses. Their results showed that when the plasma cooled, the electron density decreased due to recombination. It shows that an initial rapid increase of collision frequency. Then as the plasma heats the collision frequency goes down. After that, when the plasma cools, the collision frequency increase again due to decrease of electron density[29].

D.Jang et al. published work detailing an electron density characterization of argon plasma using THz-TDS. The plasma was characterized by the THz-TDS method. The results presented a change of electron density and a resulting phase shift of the THz pulse for different Ar gas pressures and input RF powers. An analytical model based on the ambipolar diffusion equation was used to explain the plasma density characteristics. Their experimental results and analytical results were in good agreement, but there was some deviation at electron densities higher than $5*10^{13}$ cm^{-3}[10].

K. Kang et al. presented experimental work on plasma density measurements in laser-plasmas using THz spectroscopy. The THz-TDS method was used to measure the plasma density by sending THz pulses through an inductively coupled plasma. The electron density was calculated by measuring the phase shift of the THz pulse. They used the ambipolar diffusion theoretical model to explain the experimental results, and the experimental and simulation results were consistent with each other. Their results

show that the electron density can be measured, but the ability to do so depends on the bandwidth of the incident THz radiation [30].

S. P. Jamison et al. used the THz-TDS method to measure properties of a He discharge plasma. They presented measurements of the phase shift for different plasma densities and THz pulse frequencies. The calculated and experimental amplitude were compared at different frequencies. Their work included measurements of the electron density and collision frequency of the He discharge plasma at different times [13]. N. P. Brown et al. experimentally investigated the capability of using the THz-TDS method as a plasma diagnostic. They measured the electron density and collision frequency as a function of frequency for different interaction distances of an argon inductively coupled plasma. They further studied the impact of electron temperature and applied magnetic field on boron nitride composite plasma boundaries. Their analysis showed that, if the THz pulse propagates perpendicular to a magnetic field, THz-TDS measurements are independent of the magnetic field and unaffected by electron temperature [3].

A. Ando et al. presented experimental work involving electron density measurements of an inductively coupled plasma using the THz- TDS method. They have measured the electron density of their plasma. They studied how the change of phase shift as a function of frequency changed with varying RF power. The dependence of the electron density on RF power was shown. Their results showed that both electron density and gas temperature increased with RF power. At this point, the THz-TDS method is very useful because probe methods such as Langmuir Probe cannot be used because of high gas temperature. They have theoretically shown that if the electron

density is very high, the effect of plasma size is not very sensitive as in low electron densities [12].

According to these previously reported studies, the FDTD method is an accurate method to simulate electromagnetic wave propagation. Both the Z-transform method and Auxiliary Differential Equations (ADE) methods can be used to model plasma properties such as electron density and collision frequency. Furthermore, the THz-TDS method is an accurate and widely use characterization method for plasma characterization. The properties of plasma such as absorbance, transmittance, electron density, and refractive index can be calculated using THz-TDS method.

At this point, it is important to validate the simulated plasma models. Therefore, in this study, THz pulse propagation through a plasma medium will be simulated using the FDTD method while applying the Z-transform. The THz-TDS method will be used to characterize the plasma model by calculating some plasma properties such as absorbance, transmittance, electron density and refractive index. Finally, the plasma model will be validated comparing the calculated results with the values used in the plasma simulation.

3. THEORY

This chapter focuses on a theoretical discussion of the modeling technique used in this thesis, namely the finite difference time-domain (FDTD) method. This begins with the development of what are referred to as update equations for the electromagnetic fields of a wave propagating in free space. This formalism is then expanded to consider the propagation of an electromagnetic wave through an unmagnetized plasma.

3.1 FDTD Method

The Finite Difference Time Domain (FDTD) method is a widely used technique in computational electromagnetics. This method is very popular for simulations in the microwave range, but it has been used to simulate electromagnetic waves across the spectrum. In addition to the FDTD method, there are a number of existing methods that utilize Maxwell's equations to model electromagnetic devices and phenomena including the Finite Integration Technique (FIT) and the Transmission Line Matrix (TLM) method. The time-domain FIT is equivalent to FDTD because both FDTD and FIT have a similar basic approach, the approach of TLM is unique. It uses a single spatial grid instead of interleaving electric field and magnetic field grids. In this work, only the FDTD method is considered because of the wide range of advantages such as its ability to

incorporate complex and nonlinear geometries. The construction and implementation of a FDTD model is a complex procedure, especially when there is a need to incorporate dispersive media. A medium is dispersive when waves of different frequencies travel in it at different velocities [14].

This study only utilized one-dimensional simulations i.e., propagation along one direction. When discussing the theoretical basis of the FDTD method, it is easier to understand the three-dimensional case. It is then possible to easily scale the formalism down to one dimension. This treatment starts with a consideration of these two Maxwell's equations,

$$\nabla \times E = -\mu \frac{\partial H}{\partial t} \qquad 3.1$$

$$\nabla \times H = \varepsilon \frac{\partial E}{\partial t} \qquad 3.2$$

where E is the electric field strength, H is the magnetic field strength, μ is the permeability, and ε is the permittivity. The FDTD method can be used to find update equations for electric and magnetic fields at each time step and each space point [16].

3.1.1 Finite-Difference Approximations

When the finite difference approximation is applied, continuous partial differential equations are replaced with discrete approximations. The time-derivative parts of Equations 3.1 and 3.2 can be rewritten as follows,

$$\frac{\partial H}{\partial t} = -\frac{H\left(t+\frac{\Delta t}{2}\right) - H\left(t-\frac{\Delta t}{2}\right)}{\Delta t} \quad 3.3$$

$$\frac{\partial E}{\partial t} = \frac{E(t+\Delta t) - E(t)}{\Delta t} \quad 3.4$$

The two Maxwell's equations are now written as,

$$\frac{H\left(t+\frac{\Delta t}{2}\right) - H\left(t-\frac{\Delta t}{2}\right)}{\Delta t} = -\frac{1}{\mu}\nabla \times E(t) \quad 3.5$$

$$\frac{E(t+\Delta t) - E(t)}{\Delta t} = \frac{1}{\varepsilon}\nabla \times H\left(t+\frac{\Delta t}{2}\right) \quad 3.6$$

They can be rearranged as follows,

$$H\left(t+\frac{\Delta t}{2}\right) = H\left(t-\frac{\Delta t}{2}\right) - \frac{\Delta t}{\mu}\nabla \times E(t) \quad 3.7$$

$$E(t+\Delta t) = E(t) + \frac{\Delta t}{\varepsilon}\nabla \times H\left(t+\frac{\Delta t}{2}\right) \quad 3.8$$

3.1.2 Yee Grid and Update Equations

The Yee grid is a method, that illustrates the positions of electric filed and magnetic field components [17]. This approach is a paradigm shift for solving Maxwell's equations as it illustrates the electric field and magnetic field components in both space and time, without any assumptions other than the discretization of time and space. In the Yee grid method, electric field and magnetic field vectors are assigned to a three-dimensional space grid according to Equations 3.7 and 3.8 [16].

Figure 3.2 shows the arrangement of the electric and magnetic field vectors when applied to the three-dimensional Yee grid. The magnetic field components are in the middle of the edges and the electric field components are in the center of the faces.

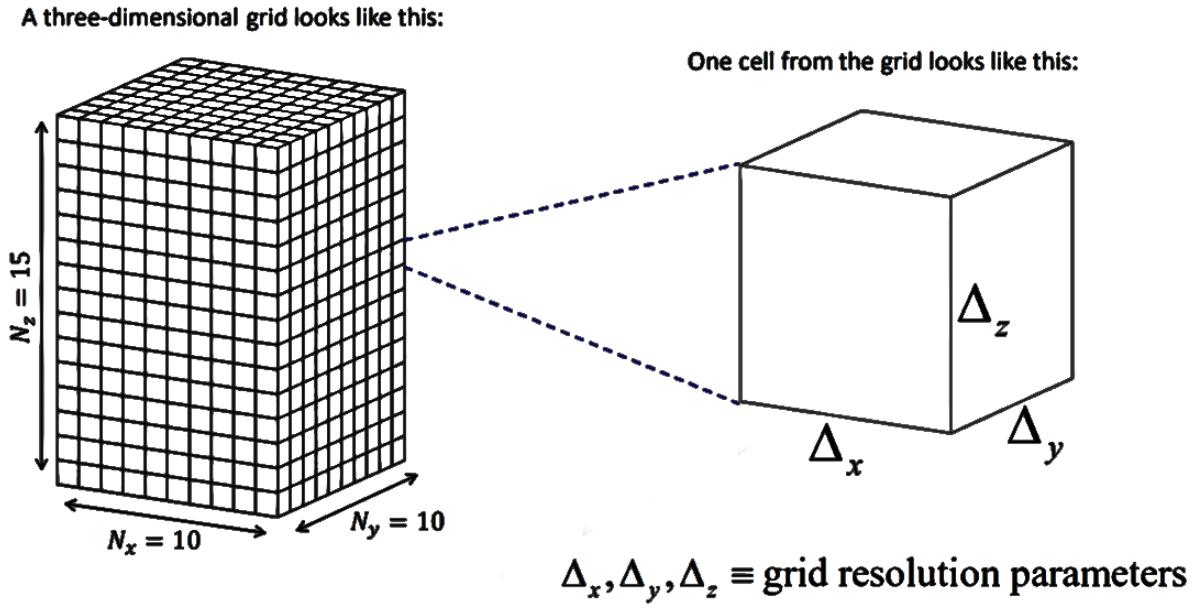

Figure 3.1: 3D Yee grid and unit cell [18].

Equation 3.2 is rewritten to consider the ABCD surface of Figure 3.2 the grid,

$$\frac{\partial H_z}{\partial y} - \frac{\partial H_y}{\partial z} = \left[\varepsilon_{xx}\frac{\partial E_x}{\partial t} + \varepsilon_{xy}\frac{\partial E_y}{\partial t} + \varepsilon_{xz}\frac{\partial E_z}{\partial t}\right] \qquad 3.9$$

The CDEF surface of the grid in the Figure 3.2 is then addressed,

$$\frac{\partial H_x}{\partial z} - \frac{\partial H_z}{\partial x} = \left[\varepsilon_{yx}\frac{\partial E_x}{\partial t} + \varepsilon_{yy}\frac{\partial E_y}{\partial t} + \varepsilon_{yz}\frac{\partial E_z}{\partial t}\right] \qquad 3.10$$

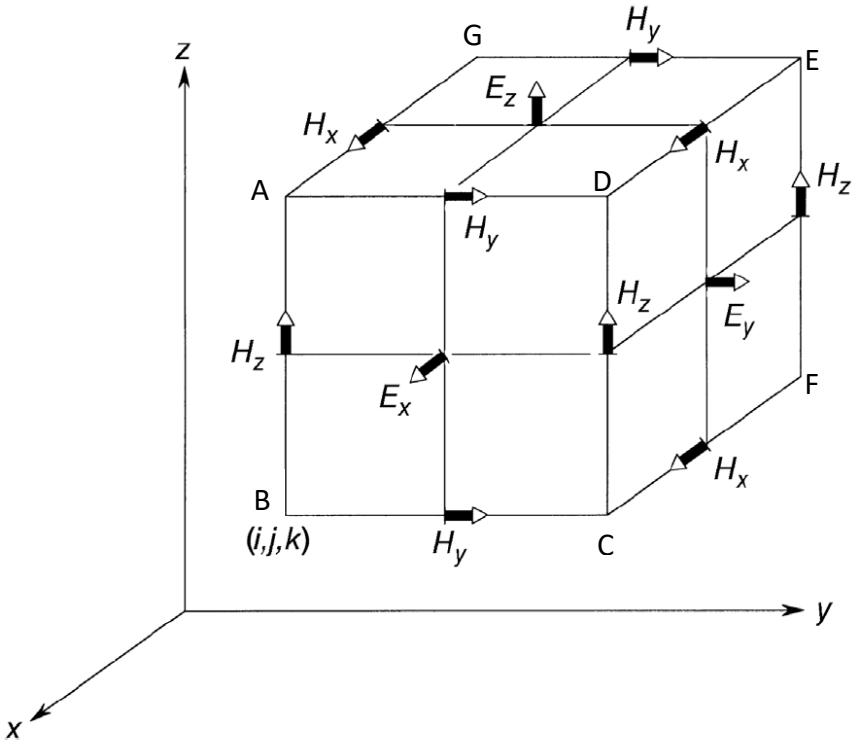

Figure 3.2: Arrangement of field component on Yee cell [19].

The ADEG surface of the grid in the Figure 3.2 is adjusted as well,

$$\frac{\partial H_y}{\partial x} - \frac{\partial H_x}{\partial y} = \left[\varepsilon_{zx}\frac{\partial E_x}{\partial t} + \varepsilon_{zy}\frac{\partial E_y}{\partial t} + \varepsilon_{zz}\frac{\partial E_z}{\partial t}\right] \qquad 3.11$$

For all three of the previous equations, the subscripts x, y and z represent the three directions in space and ∂x, ∂y,and ∂z represent the dimensions of the cubic in x, y and z directions respectively.

Using the same approach, Equation 3.1 is re-written as follows,

$$\frac{\partial E_z}{\partial y} - \frac{\partial E_y}{\partial z} = -\left[\mu_{xx}\frac{\partial H_x}{\partial t} + \mu_{xy}\frac{\partial H_y}{\partial t} + \mu_{xz}\frac{\partial H_z}{\partial t}\right] \qquad 3.12$$

$$\frac{\partial E_x}{\partial z} - \frac{\partial E_z}{\partial x} = -\left[\mu_{yx}\frac{\partial H_x}{\partial t} + \mu_{yy}\frac{\partial H_y}{\partial t} + \mu_{yz}\frac{\partial H_z}{\partial t}\right] \quad 3.13$$

$$\frac{\partial E_z}{\partial y} - \frac{\partial E_y}{\partial z} = -\left[\mu_{zx}\frac{\partial H_x}{\partial t} + \mu_{zy}\frac{\partial H_y}{\partial t} + \mu_{zz}\frac{\partial H_z}{\partial t}\right] \quad 3.14$$

If one can assume that the medium being modeled is isotropic in electromagnetic properties, it is possible to drop all of the diagonal elements from the above equations. Then Equations 3.9 – 3.14 become,

$$\frac{\partial E_z}{\partial y} - \frac{\partial E_y}{\partial z} = -\left[\mu_{xx}\frac{\partial H_x}{\partial t}\right] \quad 3.15$$

$$\frac{\partial E_x}{\partial z} - \frac{\partial E_z}{\partial x} = -\left[\mu_{yy}\frac{\partial H_y}{\partial t}\right] \quad 3.16$$

$$\frac{\partial E_z}{\partial y} - \frac{\partial E_y}{\partial z} = -\left[\mu_{zz}\frac{\partial H_z}{\partial t}\right] \quad 3.17$$

$$\frac{\partial H_z}{\partial y} - \frac{\partial H_y}{\partial z} = \left[\varepsilon_{xx}\frac{\partial E_x}{\partial t}\right] \quad 3.18$$

$$\frac{\partial H_x}{\partial z} - \frac{\partial H_z}{\partial x} = \left[\varepsilon_{yy}\frac{\partial E_y}{\partial t}\right] \quad 3.19$$

$$\frac{\partial H_y}{\partial x} - \frac{\partial H_x}{\partial y} = \left[\varepsilon_{zz}\frac{\partial E_z}{\partial t}\right] \quad 3.20$$

The finite difference approximation can now be applied to all of the partial derivatives in Equations 3.15 – 3.20. For the first part of Equation 3.15, the application of the finite difference approximation yields

$$\frac{\partial E_z}{\partial y} = \frac{E_Z^{i,j+1,k}|_t - E_Z^{i,j,k}|_t}{\Delta y} \qquad 3.21$$

where i, j, and k are the x, y and z coordinates of position of the cubic Yee cell in Figure 3.1, t is time, and Δy is length of the cell in the y-direction. Thus, $E_Z^{i,j+1,k}|_t$ is the z-direction electric field component of the cell that, in the right side of the (i,j+1,k) cell at time t. $E_Z^{i,j,k}|_t$ is the z-direction electric field component of the (I,j,k) cell at time t. $E_Z^{i,j+1,k}|_t - E_Z^{i,j,k}|_t$ is the difference of of the z-direction electric fields in the (i,j,k) cell and (i,j+1,k) cells.

The finite difference approximation is now applied to the second part of Equation 3.15

$$\frac{\partial E_y}{\partial z} = \frac{E_y^{i,j,k+1}|_t - E_y^{i,j,k}|_t}{\Delta z} \qquad 3.22$$

Equations 3.21, 3.22 and 3.3 are all substituted together into Equation 3.15. The final equation then becomes,

$$\frac{E_Z^{i,j+1,k}|_t - E_Z^{i,j,k}|_t}{\Delta y} - \frac{E_y^{i,j,k+1}|_t - E_y^{i,j,k}|_t}{\Delta z} = -\mu_{xx}\frac{H_x^{i,j,k}|_{t+\frac{\Delta t}{2}} - H_x^{i,j,k}|_{t-\frac{\Delta t}{2}}}{\Delta t} \qquad 3.23$$

This same method is applied to Equations 3.16 – 3.20.

$$\frac{E_x^{i,j,k+1}|_t - E_x^{i,j,k}|_t}{\Delta z} - \frac{E_y^{i+1,j,k}|_t - E_y^{i,j,k}|_t}{\Delta x} = -\mu_{yy}\frac{H_y^{i,j,k}|_{t+\frac{\Delta t}{2}} - H_y^{i,j,k}|_{t-\frac{\Delta t}{2}}}{\Delta t} \quad 3.24$$

$$\frac{E_y^{i,j+1,k}|_t - E_y^{i,j,k}|_t}{\Delta x} - \frac{E_x^{i,j+1,k}|_t - E_x^{i,j,k}|_t}{\Delta y} = -\mu_{zz}\frac{H_z^{i,j,k}|_{t+\frac{\Delta t}{2}} - H_z^{i,j,k}|_{t-\frac{\Delta t}{2}}}{\Delta t} \quad 3.25$$

$$\frac{H_Z^{i,j,k}|_{t+\frac{\Delta t}{2}} - H_Z^{i,j-1,k}|_{t+\frac{\Delta t}{2}}}{\Delta y} - \frac{H_y^{i,j,k}|_{t+\frac{\Delta t}{2}} - H_y^{i,j,k-1}|_{t+\frac{\Delta t}{2}}}{\Delta z} = \varepsilon_{xx}\frac{E_x^{i,j,k}|_{t+\Delta t} - E_x^{i,j,k}|_t}{\Delta t} \quad 3.26$$

$$\frac{H_x^{i,j,k}|_{t+\frac{\Delta t}{2}} - H_x^{i,j,k-1}|_{t+\frac{\Delta t}{2}}}{\Delta z} - \frac{H_z^{i,j,k}|_{t+\frac{\Delta t}{2}} - H_z^{i-1,j,k}|_{t+\frac{\Delta t}{2}}}{\Delta x} = \varepsilon_{yy}\frac{E_y^{i,j,k}|_{t+\Delta t} - E_y^{i,j,k}|_t}{\Delta t} \quad 3.27$$

$$\frac{H_y^{i,j,k}|_{t+\frac{\Delta t}{2}} - H_y^{i-1,j-1,k}|_{t+\frac{\Delta t}{2}}}{\Delta x} - \frac{H_x^{i,j,k}|_{t+\frac{\Delta t}{2}} - H_x^{i,j-1,k}|_{t+\frac{\Delta t}{2}}}{\Delta y} = \varepsilon_{zz}\frac{E_z^{i,j,k}|_{t+\Delta t} - E_z^{i,j,k}|_t}{\Delta t} \quad 3.28$$

These six equations 3.23 – 3.28 can be used to calculate the electric field at the later time based on the knowledge of the previous electric field and perpendicular magnetic field. The same can be said for the new magnetic field. In other words, these equations update the electric field and magnetic field definition for a propagating electromagnetic wave. Therefore, these equations are referred to as the update equations for a three-dimensional space. For a three-dimensional simulation, it is necessary to utilize all six equations in order to update the time evolution of the electric field and magnetic fields in all three directions.

The simulation work presented herein considers a 1-dimensional wave propagating in the z-direction and utilizes the following plane-wave approximation,

$$\frac{\partial}{\partial x} = \frac{\partial}{\partial y} = 0 \tag{3.29}$$

Equations 3.23 – 3.28 are reduced to the following four equations

$$-\frac{E_y^{i,j,k+1}|_t - E_y^{i,j,k}|_t}{\Delta z} = -\mu_{xx}\frac{H_x^{i,j,k}|_{t+\frac{\Delta t}{2}} - H_x^{i,j,k}|_{t-\frac{\Delta t}{2}}}{\Delta t} \tag{3.30}$$

$$\frac{E_x^{i,j,k+1}|_t - E_x^{i,j,k}|_t}{\Delta z} = -\mu_{yy}\frac{H_y^{i,j,k}|_{t+\frac{\Delta t}{2}} - H_y^{i,j,k}|_{t-\frac{\Delta t}{2}}}{\Delta t} \tag{3.31}$$

$$-\frac{H_y^{i,j,k}|_{t+\frac{\Delta t}{2}} - H_y^{i,j,k-1}|_{t+\frac{\Delta t}{2}}}{\Delta z} = \varepsilon_{xx}\frac{E_x^{i,j,k}|_{t+\Delta t} - E_x^{i,j,k}|_t}{\Delta t} \tag{3.32}$$

$$\frac{H_x^{i,j,k}|_{t+\frac{\Delta t}{2}} - H_x^{i,j,k-1}|_{t+\frac{\Delta t}{2}}}{\Delta z} = \varepsilon_{yy}\frac{E_y^{i,j,k}|_{t+\Delta t} - E_y^{i,j,k}|_t}{\Delta t} \tag{3.33}$$

Since the medium has been defined as being isotropic, it is assumed that the electric field vector is contained in the x-direction and the magnetic field in the y-direction, Equations 3.30 and 3.33 are eliminated and 3.31 is rearranged as

$$E_x^{i,j,k}|_{t+\Delta t} = E_x^{i,j,k}|_t - \left(\frac{\Delta t}{\varepsilon_{xx}}\right)\left(\frac{H_y^{i,j,k}|_{t+\frac{\Delta t}{2}} - H_y^{i,j,k-1}|_{t+\frac{\Delta t}{2}}}{\Delta z}\right) \qquad 3.34$$

It can be seen that the above equation is not dependent on the i and j indices such that they can be removed yielding a simplified update equation for the electric field in the x-direction,

$$E_x^k|_{t+\Delta t} = E_x^k|_t - \left(\frac{\Delta t}{\varepsilon_{xx}\Delta z}\right)\left(H_y^k|_{t+\frac{\Delta t}{2}} - H_y^{k-1}|_{t+\frac{\Delta t}{2}}\right) \qquad 3.35$$

The same approach yields a one-dimensional update equation for the magnetic field,

$$H_y^k|_{t+\frac{\Delta t}{2}} = H_y^k|_{t-\frac{\Delta t}{2}} - \left(\frac{\Delta t}{\mu_{yy}\Delta z}\right)(E_x^{k+1}|_t - E_x^k|_t) \qquad 3.36$$

In Equations 3.35 and 3.36, $\left(\frac{\Delta t}{\varepsilon_{xx}\,\Delta z}\right)$ and $\left(\frac{\Delta t}{\mu_{yy}\,\Delta z}\right)$ are referred to as the Update coefficients [20]. These two coefficients are very similar, but one coefficient depends on ε_{xx} and the other on μ_{yy}. As a result of this, the magnitude of the electric field and magnetic fields will differ by several orders of magnitude [20]. A new electric field variable is defined as,

$$\tilde{E}_x^k = \sqrt{\frac{\varepsilon_{xx}}{\mu_{yy}}} E_x^k \tag{3.37}$$

The two updates equations are hence modified,

$$\tilde{E}_x^k|_{t+\Delta t} = \tilde{E}_x^k|_t - \left(\frac{\Delta t}{\sqrt{\varepsilon_{xx}\,\mu_{yy}}\Delta z}\right)\left(H_y^k|_{t+\frac{\Delta t}{2}} - H_y^{k-1}|_{t+\frac{\Delta t}{2}}\right) \tag{3.38}$$

$$H_y^k|_{t+\frac{\Delta t}{2}} = H_y^k|_{t-\frac{\Delta t}{2}} - \left(\frac{\Delta t}{\sqrt{\varepsilon_{xx}\,\mu_{yy}}\Delta z}\right)\left(\tilde{E}_x^{k+1}|_t - \tilde{E}_x^k|_t\right) \tag{3.39}$$

For numerical stability of time stepping update equations Δt should be chosen according to the Courant condition [22]. The Courant condition states that Δt and Δz should be chosen as,

$$\Delta t \leq \frac{\Delta z}{\sqrt{3}c_{max}} \tag{3.40}$$

where c_{max} is the maximum wave velocity within the model. In this case c_{max} should be the velocity of light in the vacuum(c). Therefore, Δt and Δz should be chosen as,

$$\Delta t \leq \frac{\Delta z}{\sqrt{3}c} \tag{3.41}$$

$Usually$, Δt chosen as $\Delta t = \frac{\Delta z}{2C}$ in most of the FDTD simulations [23].

The two update equations are now defined as,

$$\tilde{E}_x^k|_{t+\Delta t} = \tilde{E}_x^k|_t - \left(\frac{1}{2}\right)\left(H_y^k|_{t+\frac{\Delta t}{2}} - H_y^{k-1}|_{t+\frac{\Delta t}{2}}\right) \tag{3.42}$$

$$H_y^k|_{t+\frac{\Delta t}{2}} = H_y^k|_{t-\frac{\Delta t}{2}} - \left(\frac{1}{2}\right)\left(\tilde{E}_x^{k+1}|_t - \tilde{E}_x^k|_t\right) \quad 3.43$$

3.2 Simulations of Unmagnetized Plasma

In Section 3.1, update equations were developed for the electric field and magnetic fields in vacuum. In this section, the update equations for propagation in a plasma medium are developed. As mentioned in Chapter 1, plasmas do not affect the magnetic field of an electromagnetic wave in the absence of an applied external magnetic field. Therefore, for the case of an unmagnetized plasma, the magnetic field update equation does not require any modifications. The permittivity of an unmagnetized plasma is given in Equation 1.6,

$$\varepsilon_r = 1 - \frac{\omega_p^2}{(\omega^2 - i\omega\nu_c)}$$

Using the partial fraction method, one can rewrite the above equation as follows,

$$\varepsilon_r = 1 + \frac{\frac{\omega_p^2}{\nu_c}}{i\omega} - \frac{\frac{\omega_p^2}{\nu_c}}{\nu_c + i\omega} \quad 3.44$$

There are a number of ways to perform a FDTD simulation of propagation through a plasma, such the Auxiliary Differential Equation (ADE) method and the Z-transform method [15]. This study utilizes the Z-transform method. The Z-transform is a

mathematical technique widely used in signal processing to analyze time-domain signals having complex properties in the frequency domain. The Z-transform for discrete time signals is similar to the Laplace transform for continuous time signals. Both the Laplace transform and Z-transform have a similar relationship to the Fourier transform [24]. Table 3.1 depicts several of the Z- transforms that were used in this section. Applying Z-transforms to Equation 3.44,

$$\varepsilon_r(z) = \frac{1}{\Delta t} + \frac{\frac{\omega_p^2}{\nu_c}}{1 - z^{-1}} - \frac{\frac{\omega_p^2}{\nu_c}}{1 - e^{-\nu_c \Delta t} z^{-1}} \qquad 3.45$$

Time Domain	Frequency Domain	Z Domain
δt	1	$\frac{1}{\Delta t}$
u(t)	$\frac{1}{i\omega}$	$\frac{1}{1 - z^{-1}}$
$e^{-\alpha t}$ u(t)	$\frac{1}{i\omega + \alpha}$	$\frac{1}{1 - e^{-\alpha \Delta t} z^{-1}}$

Table 3.1: Some Z transforms [21].

In electrodynamics, the electric flux density is defined as

$$D = \varepsilon_r \tilde{E} \qquad 3.46$$

where D is the electric flux density, $\varepsilon_r$is the permittivity, and $\tilde{E}$ is the complex electric field intensity. Using the convolution theorem, the Z-transform of the above equation can be written as [21],

$$D(z) = \varepsilon_r(z)\, E(z).\Delta t \qquad 3.47$$

Substituting the Equations 3.45 to 3.47 yields,

$$D(z) = E(z) + \frac{\omega_p^2 \Delta t}{\nu_c}\left[\frac{1}{1 - z^{-1}} - \frac{1}{1 - e^{-\nu_c \Delta t} z^{-1}}\right] E(z) \qquad 3.48$$

$$D(z) \qquad 3.49$$

$$= E(z) + \frac{\omega_p^2 \Delta t}{\nu_c}\left[\frac{(1 - e^{-\nu_c \Delta t})\, z^{-1}}{1 - (1 + e^{-\nu_c \Delta t})\, z^{-1} + e^{-\nu_c \Delta t} z^{-2}}\right] E(z)$$

An auxiliary term can be defined as ($S(z)$) ,

$$S(z) = \frac{\omega_p^2 \Delta t}{\nu_c}\left[\frac{1 - e^{-\nu_c \Delta t}}{1 - (1 + e^{-\nu_c \Delta t})\, z^{-1} + e^{-\nu_c \Delta t} z^{-2}}\right] E(z) \qquad 3.50$$

One can rewrite the Equations 3.49 in terms of $S(z)$ and rearrange as follows

$$E(z) = D(z) - z^{-1} S(z) \qquad 3.51$$

Equation (3.50) can be rearranged

$$S(z) = (1 + e^{-\nu_c \Delta t})\, z^{-1} S(z) - e^{-\nu_c \Delta t}\, z^{-2} S(z) \qquad 3.52$$

$$+ \frac{\omega_p^2 \Delta t}{\nu_c}(1 - e^{-\nu_c \Delta t}) E(z)$$

Equations 3.51 and 3.52 can be used to determine the electric field of wave propagating in a plasma medium. When calculating the $S(z)$ value, it requires the $S(z)$ value in previous step. Equations 3.51 and 3.52 are the update equations for an electric field in

plasma. As mentioned previously, a plasma medium does not affect the magnetic field of a propagating wave. This is realized as the magnetic field update equation in a plasma is the same as the magnetic field update equation in free space. Therefore, Equation 3.43 can be used as magnetic field update equation in plasma [21].

Finally, the update equations for the electric field (Equation 3.42) and magnetic field (Equation 3.43) in free space are simulated using MATLAB (Appendix 1). Equations 3.51 and 3.52 are used to introduce the plasma medium. The variation of the electric field is recorded in the time domain for varying plasma properties. The effects of the plasma properties on the amplitude and phase of the electric field of a propagating electromagnetic wave is discussed in the following Results and Discussion chapter.

4. RESULTS AND DISCUSSION

The previous chapters discussed both the FDTD technique as well as the experimental technique of terahertz time-domain spectroscopy. This chapter presents results of FDTD modeling of terahertz pulses propagating through a plasma medium. A data analysis technique used in experimental time-domain measurements is applied to the modeling data as a tool to verify the simulation results. This is used to extract from the simulation data plasma parameters such as the electron density. The "extracted" parameters are compared to the original values of electron density that served as input parameters for the simulation.

4.1 Physical design

The simulation domain is described by Figure 4.1. The FDTD simulated pulse travels in the z-direction where d is the thickness of the plasma interaction medium, Z_1 is the distance traveled by the pulse prior to the plasma medium, and Z_2 is the distance traveled by the pulse after the plasma medium. Z_1 and Z_2 are selected as 2 mm and 1 mm respectively.

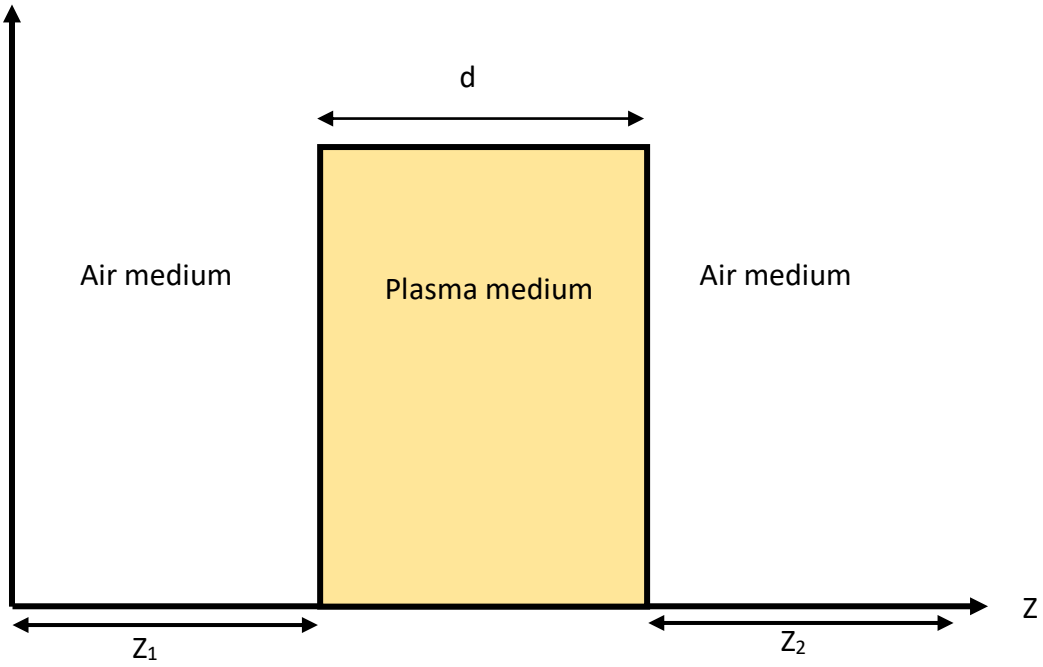

Figure 4.1: 1D FDTD simulation environment.

Figure 4.2 shows the incident pulse that used in the simulation. For all of the FDTD simulation results reported here, a time-domain pulse was the source of electromagnetic radiation. In the time-domain, the duration of the pulse was approximately 2.0 picoseconds, corresponding to the equivalent in the frequency domain of a center near 0.5 THz spanning from 0.1 to just above 2.0 THz.

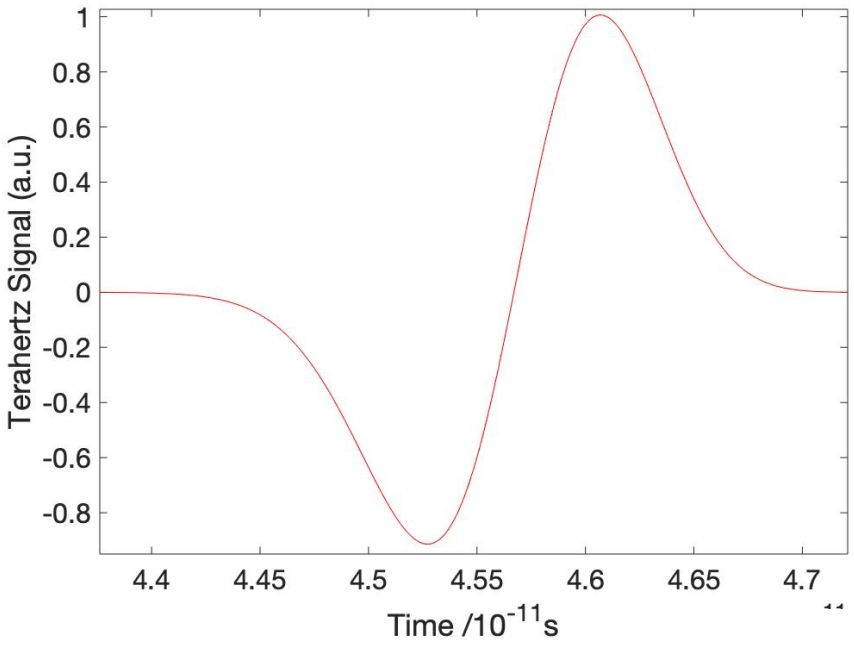

Figure 4.2(a): Incident electromagnetic pulse represented in the time-domain

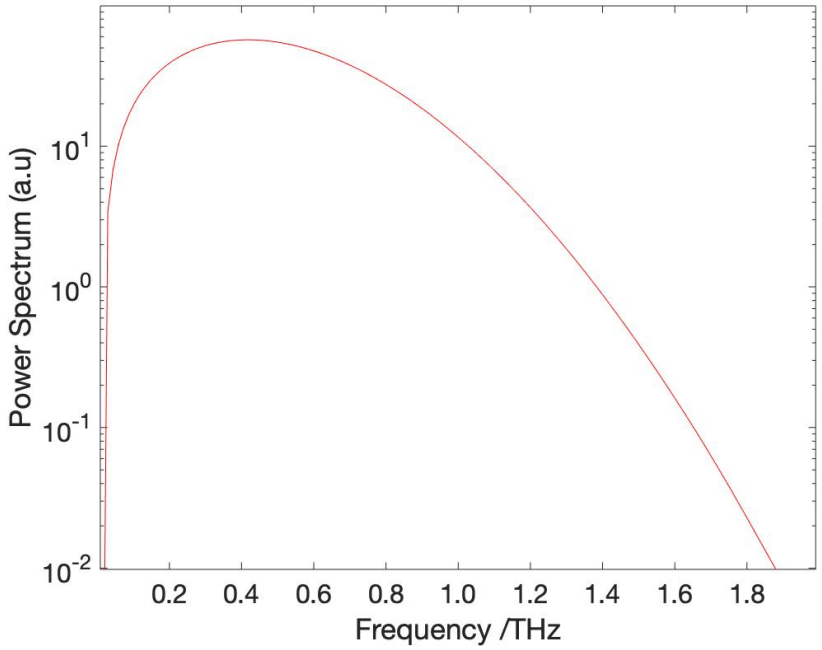

Figure 4.2(b): Incident electromagnetic pulse represented in the frequency-domain.

All of the results discussed in this chapter are taken using this pulse as the source.

4.2 Simulation Parameters and The Procedure

As the main simulation parameter, the Yee grid size(Δz) is chosen to be 0.1 μm. The size of the time element is chosen to satisfy the Courant condition as explained in Chapter 3, which is $\Delta t = \frac{\Delta z}{2C}$. Figure 4.3 shows the flow chart of the procedure of this study.

4.3 Effect of thickness of the plasma medium.

In this section, the dependence of the plasma medium interaction distance on the transmitted intensity of the THz pulse is modeled. Figure 4.4 is a graph of the intensity of the transmitted pulse versus the interaction length of the plasma medium for 4 separate simulation models, each having a different defined input electron density. All values in this plot represent the intensity at 0.5 THz as taken from frequency-domain data resulting from a Fast Fourier Transform of the modeled output pulse. All of these reported simulation results are based on the assumption that the collision frequency is 1% of electron density value in cm^{-3}. The implications of this will be discussed later.

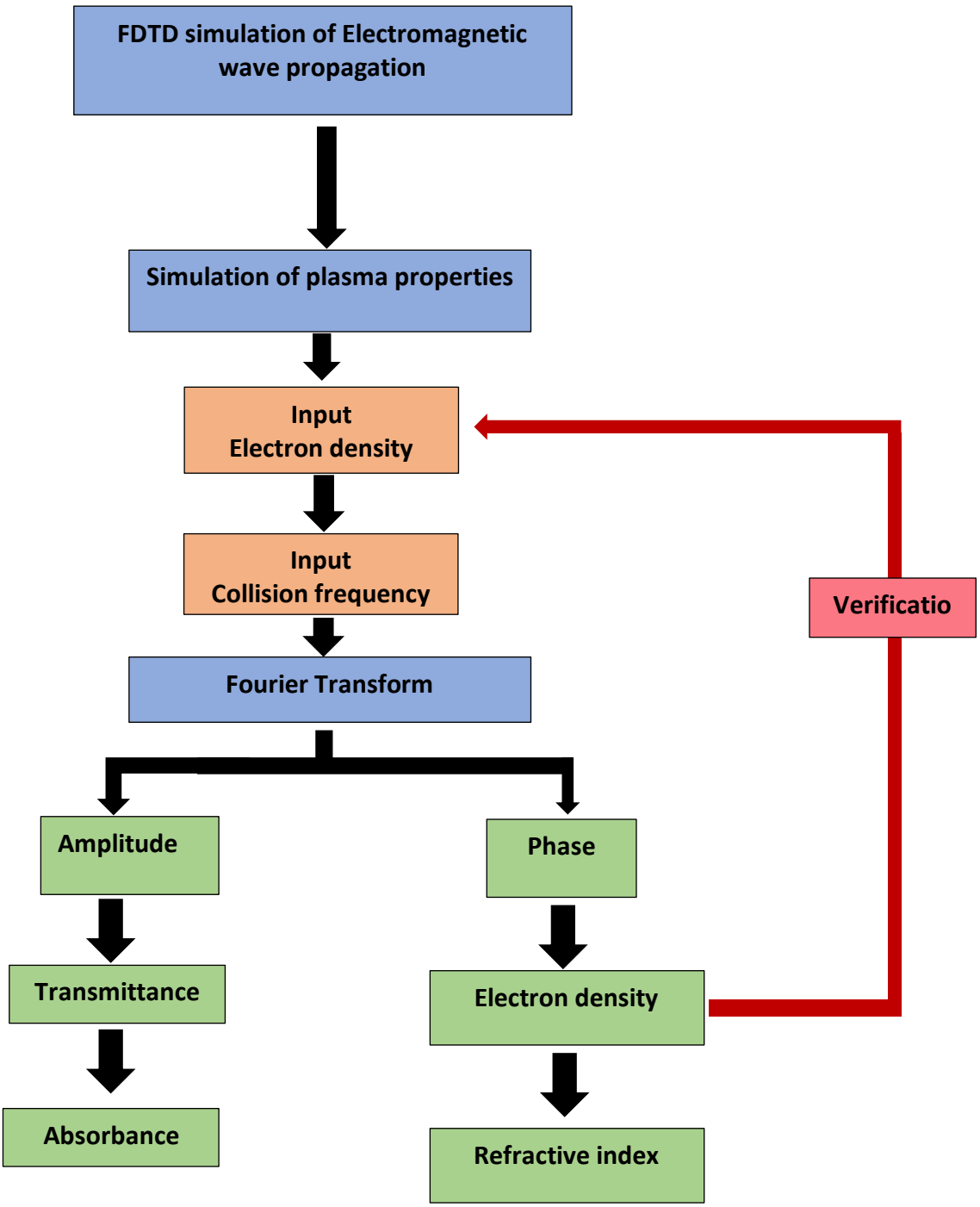

Figure 4.3: Flow chart of the procedure.

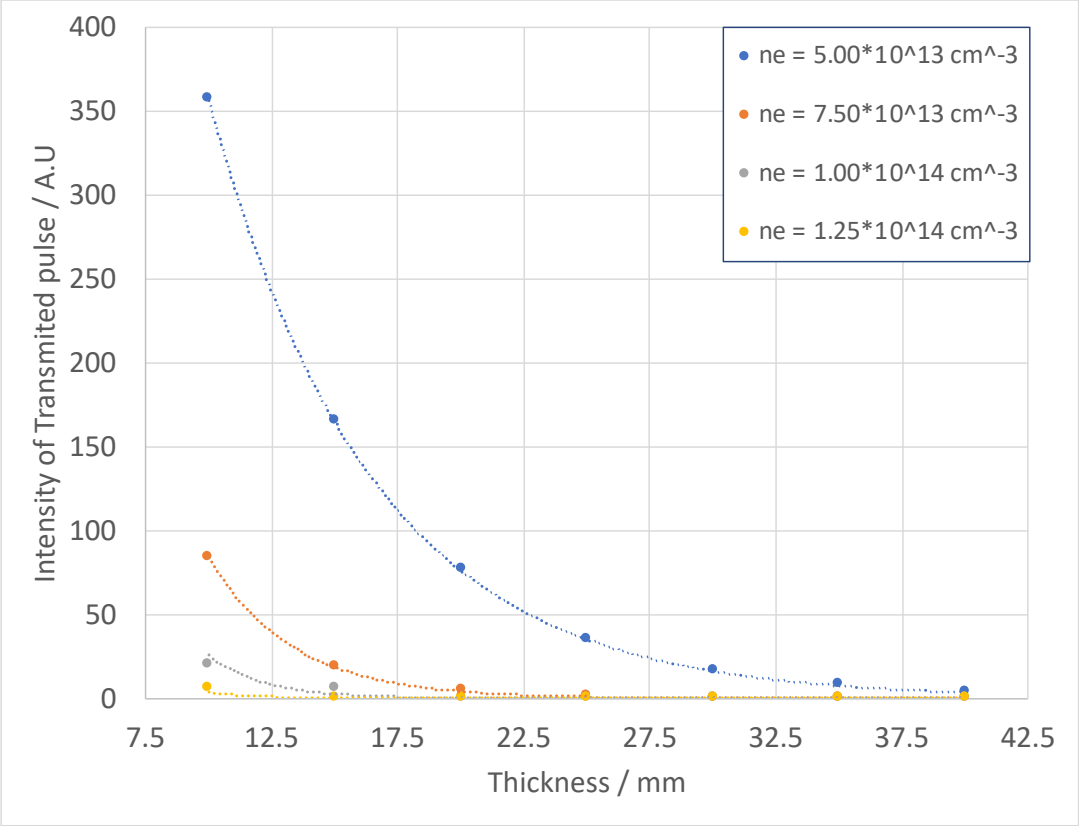

Figure 4.4: The dependence of the transmitted pulse intensity at 0.5 THz as a function of a variety of plasma medium interaction distances for differing input electron densities.

The dotted lines in Figure 4.4 represent exponential curve fits of the data points for each defined electron density. All four data sets match well to an exponential fit. Therefore, the model matches expectations as it is expected that the intensity of the transmitted pulse is exponentially dependent on the plasma interaction distance as defined by Equation (4.1)

$$I_T = I_0 e^{-\alpha d} \qquad 4.1$$

where I_T is the intensity of the transmitted pulse, I_0 is the intensity of the incident pulse, d is the interaction length of the plasma medium, and α is the attenuation coefficient [31]. Intensities are calculated using the square of the amplitude. Using this, it is possible to extract a value for the attenuation coefficient from the curve-fitted data. Table 4.1 shows those calculated α values corresponding to each input electron density from Figure 4.5.

Electron density / cm^{-3}	Attenuation coefficient / cm^{-1}
$5.00*10^{13}$	1.15
$7.50*10^{13}$	3.01
$1.00*10^{14}$	4.51
$1.25*10^{14}$	5.14

Table 4.1: Electron density and attenuation coefficients.

The attenuation coefficient is a measurement of absorption and scattering losses from the unit thickness of a material. Figure 4.5 is a graph of the simulated attenuation coefficient versus the input electron density. The results show that the attenuation coefficient increases with the electron density as expected. Because high number of electron can highly attenuate the electromagnetic wave.

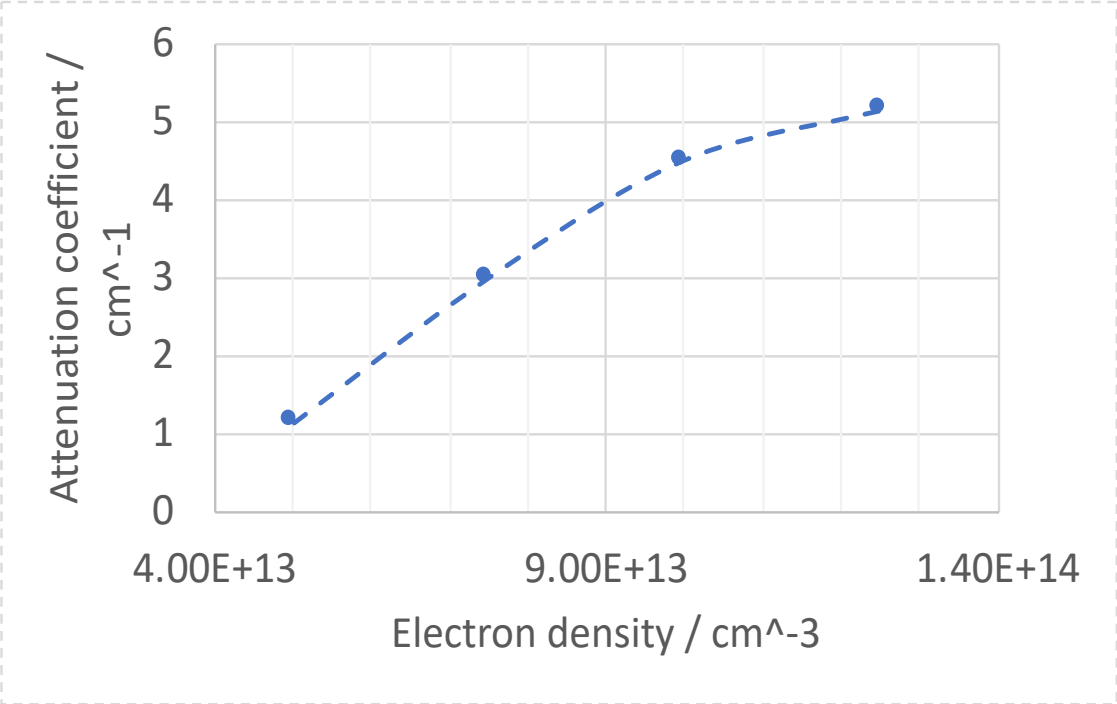

Figure 4.5: Attenuation Coefficient versus Electron Density at 0.5 THz.

Many of the optical properties of plasmas are highly dependent on the plasma frequency. Light that is at a frequency below the plasma frequency is blocked by the plasma medium while frequencies higher than that are transmitted. As described in Chapter 1, the plasma frequency can be calculated using Equation 1.1 and Table 4.2 shows the values of the plasma frequency were determined using Equation 1.1.

$$\omega_p = \sqrt{\frac{n_e e^2}{\varepsilon_0 m}} \qquad 1.1$$

Therefore, increasing electron density should increase the attenuation as a result of the plasma frequency increasing.

Electron density / cm^{-3}	Plasma frequency / THz
$5.00*10^{13}$	0.06
$7.50*10^{13}$	0.08
$1.00*10^{14}$	0.09
$1.25*10^{14}$	0.10
$1.50*10^{14}$	0.11

Table 4.2: Calculated plasma frequency values for different electron density values

4.4 Transmittance and Absorbance

The transmittance is defined as the ratio of the incident and transmitted radiation intensity as shown in Equation 4.2.

$$T = \frac{I_T}{I_0} \qquad 4.2$$

where I_T is the intensity of transmitted radiation and I_0 is the intensity of incident radiation.

Figure 4.5(a) depicts the variation of transmittance with frequency for five different input electron density values. From that figure, we can clearly see, transmittance increasing with frequency and with electron density.

These results also agree with the explanation in Section 4.3. For this section, the plasma frequencies are very low compared to the incident pulse frequency. Low frequencies show very low transmittance, and the high frequencies show very high transmittance. This is because low frequencies are near the plasma frequency values and higher frequency values are very much higher than the plasma frequency values. Transmittance decreases as the electron density increases. Higher electron density values mean a higher plasma frequency and that plasma frequency value is closer to the frequency of incident pulse. Therefore, high electron density mediums have low transmittance and low electron density mediums have high transmittance.

Absorbance is defined on a log scale as follows,

$$A = -log_{10}\left(\frac{I_T}{I_0}\right) \tag{4.3}$$

where I_T is the intensity of transmitted radiation and I_0 is the intensity of incident radiation. Calculated absorbance values from the simulation data are shown in Figure 4.6 (b). It shows the inverse behavior of the transmittance as expected.

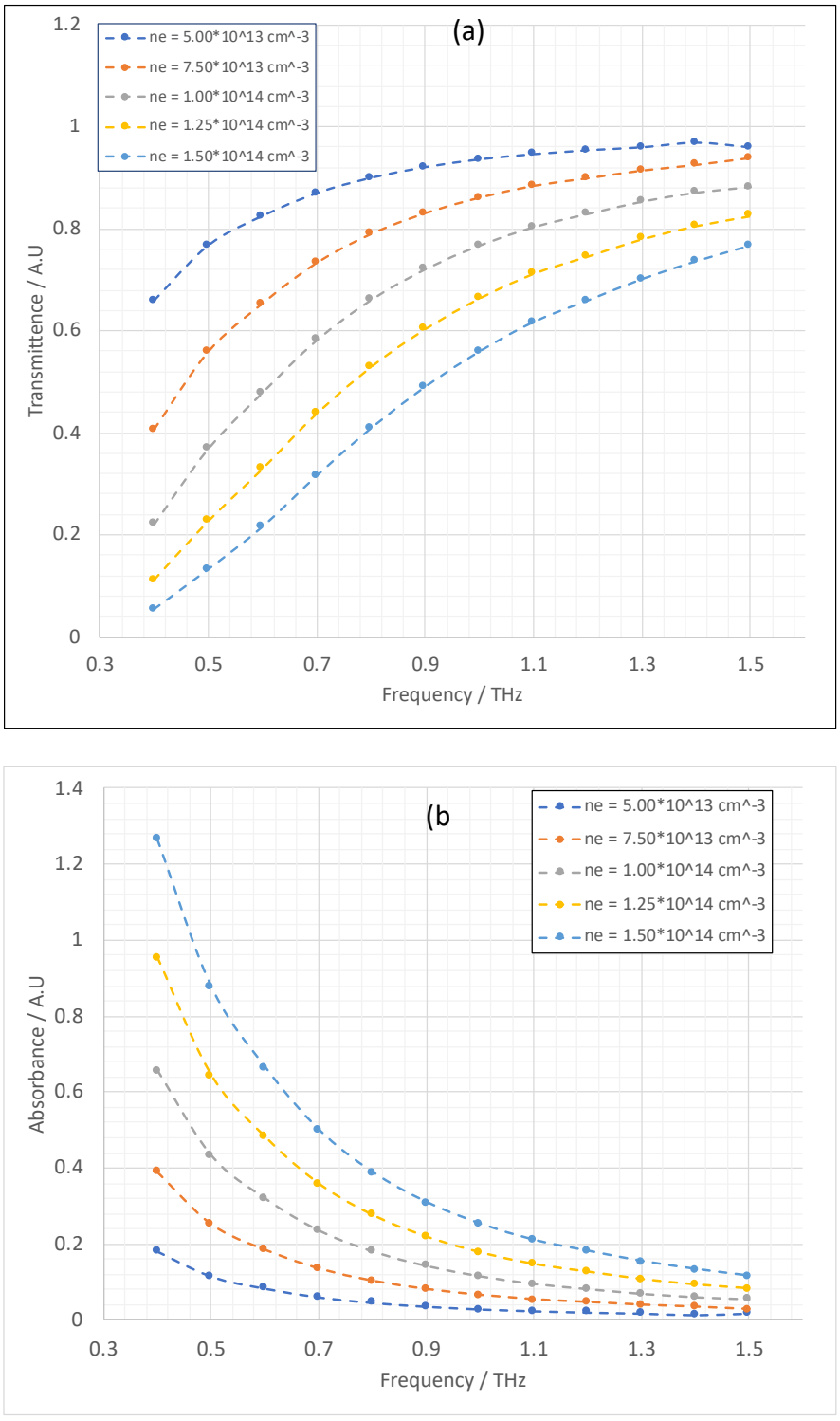

Figure 4.6: Variation of transmittance (a) and absorbance (b) values with frequency and electron density.

4.5 Effect of electron density

The electron density is one of the most important plasma parameters. Figure 4.7 shows the signal after propagating through a 10 mm thick plasma medium, represented in both the time-domain and frequency-domain. The effect of collision frequency is very low compared to the effect of electron density. The collision frequency should increase with electron density. In this study, it was assumed that the collision frequency of the plasma increased with increasing electron density such that the value of the collision frequency was 1% of the electron density value in cm^{-3} [3].

Important features can be observed in the simulation results presented in Figure 4.7. First, in the time-domain graph, the reference pulse (pulse that propagated through an equivalent amount of air) arrived at the end of the simulation domain before other pulses. Pulses that traveled through the plasma with high electron densities took longer to reach that point than reference pulse. This result implies, with increasing electron density, the pulse velocity decreases inside the plasma medium. Figure 4.7 (a) further shows that the amplitude of transmitted pulses decreases with increasing electron density. This agrees with the transmittance and absorbance results.

One of the most important features in Figure 4.7 (a) is that the THz pulse starts to change its shape (amplitude and duration of the pulse). Amplitude of the pulse is decreased with the electron density increase and duration of a single pulse also decrease with the electron density increase.

From the frequency domain plot of Figure 4.7 (b), it can be seen that the center frequency (Frequency with maximum intensity) has shifted to higher frequencies with

increasing electron densities and the bandwidth of the pulse is decreased. The reason for this shifting is that the plasma absorbs/scatters low frequency radiation and transmits most of the light at high frequencies. Therefore, these results agree with the concept of plasma frequency.

This analysis so far has only considered the amplitude data, but it is important to remember that the Fourier transform of the data from the time-domain to the frequency-domain yields both amplitude and phase information. Studying the phase change can allow one to calculate plasma properties more robustly such as the electron density and effective refractive index. Figure 4.8 shows the extracted change of phase for different electron densities.

As explained in Chapter 1, Equation 1.27 can be used to calculate the electron density of the plasma from the change of phase. Figure 4.9 shows a comparison of the input electron density values defined in the simulation model and the calculated electron density values from the change of phase (Figure 4.8) at 0.5 THz.

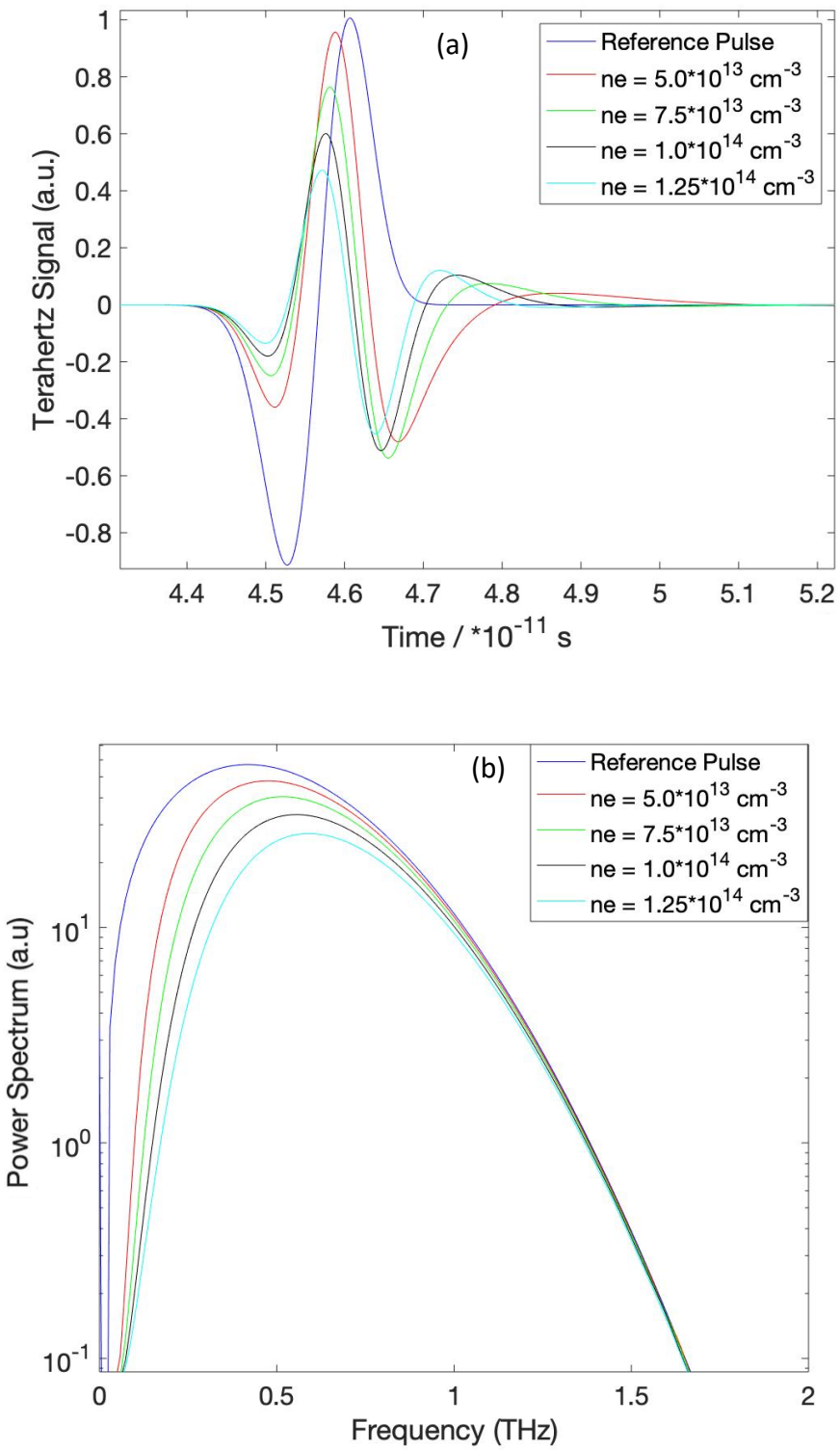

Figure 4.7: Transmitted signal in time domain (a) and frequency domain (b) for different electron densities.

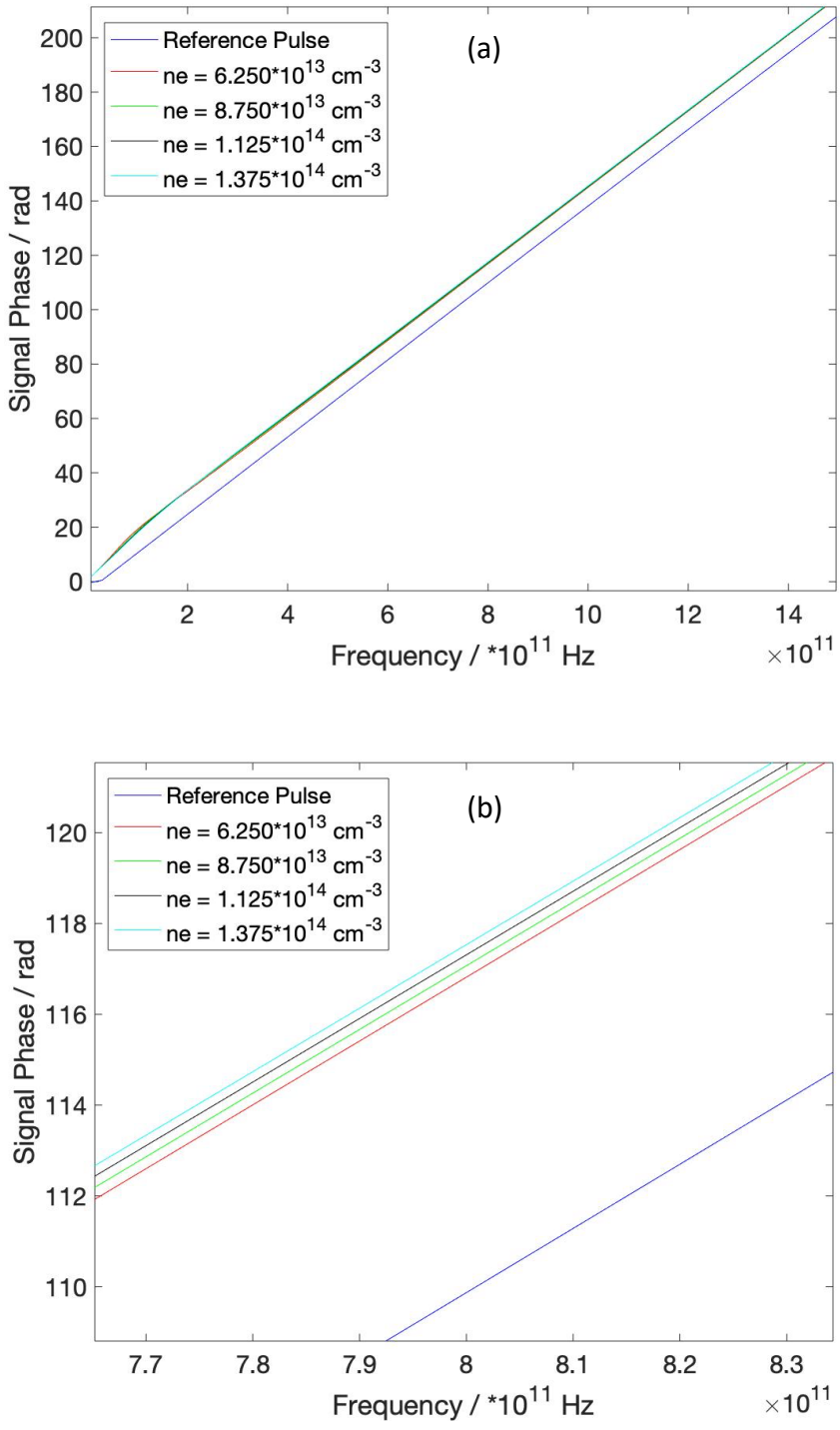

Figure 4.8: The phase of the transmitted pulse with different plasma electron densities(a), and magnified graph around 0.8THz regain(b).

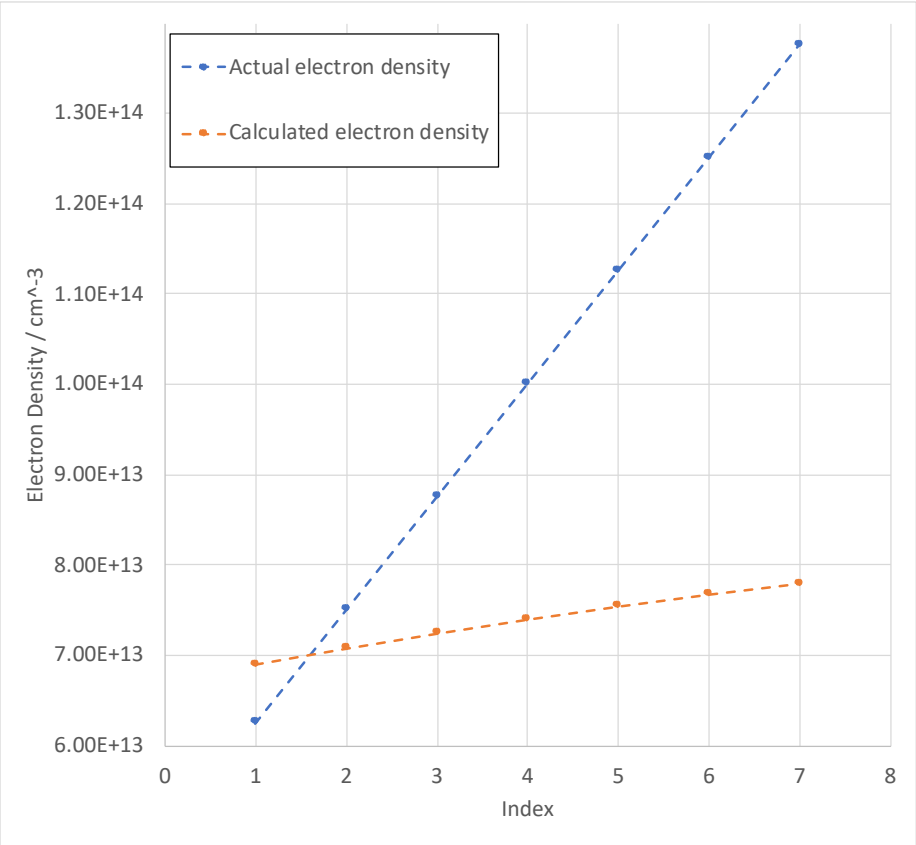

Figure 4.9: Comparison of actual electron density and calculated electron density.

From Figure 4.9, it can be seen that, even though there is agreement for values of low electron density, the difference between the actual and calculated values increases with increasing electron density. One reason for that deviation may be the assumption that was made for the collision frequency. The relationship between electron density and collision frequency might not be a linear relationship as was assumed. The time resolution of the FDTD simulation could be a cause of this discrepancy. To further study this deviation, one can compare the actual and calculated values using Equation 4.4. Figure 4.10 shows this calculated percent error as a function of frequency for different electron densities.

$$Percent\ error\ = \left|\frac{Actual\ value\ -\ Calculated\ value}{Actual\ value}\right| \times 100\% \qquad 4.4$$

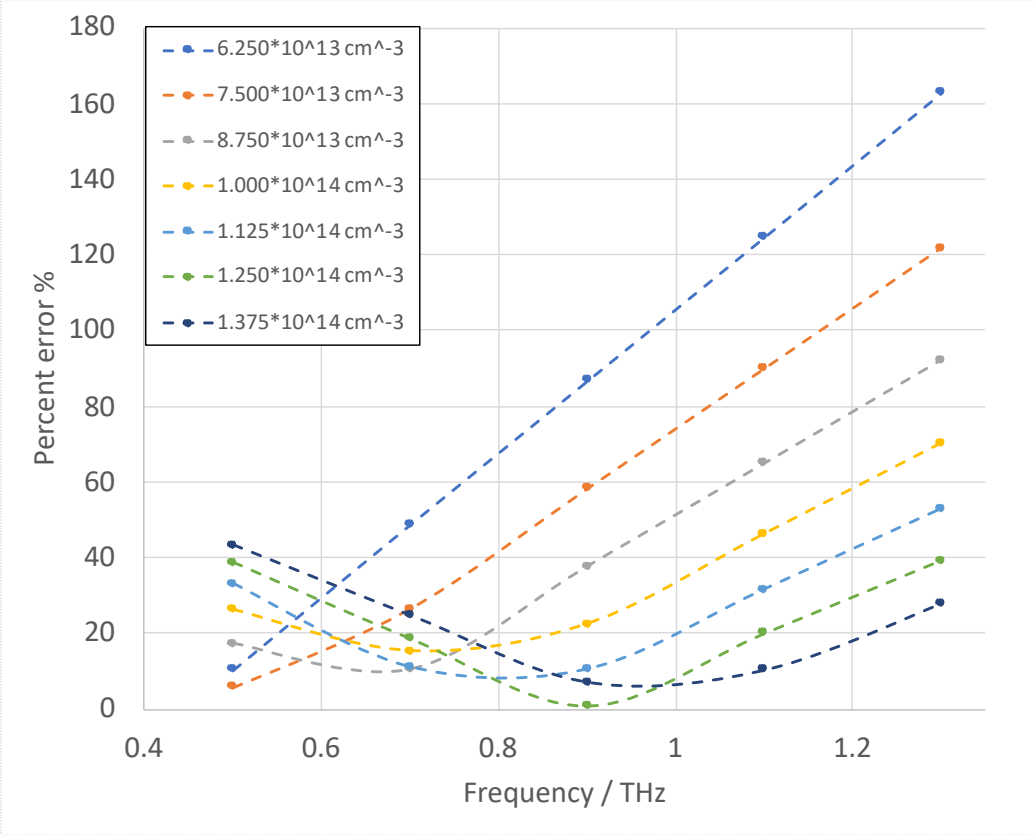

Figure 4.10: Variation of percent error of calculated electron density values with frequency.

For each electron densities, the percent error is significantly higher at high frequency values. These large errors at high frequencies could be evidence that the time resolution of the simulations was not low enough. The size of the time element should be very small compared to the period (1/frequency) of the signal in order to get more accurate results. In the low frequency range, for some electron densities, the percent error

increases with frequency while for other electron density values, the percent error decreases to a minimum and then increases again.

Figure 4.11 shows how this percent error changes as the time resolution of the simulation is manipulated. The data shown is this figure is the percent error at the specified frequencies. Percent error values at 0.7 THz, 0.9 THz and 1.1 THz are decreasing as the size of the time element is lowered (increasing the time resolution), which can be expected. This suggests that the high deviation of the calculated electron density at higher frequencies is possibly due to the low time resolution of the simulation. However, the data at 0.5 THz pulse does not support this reasoning. This discrepancy might be due to the high absorption present at 0.5 THz.

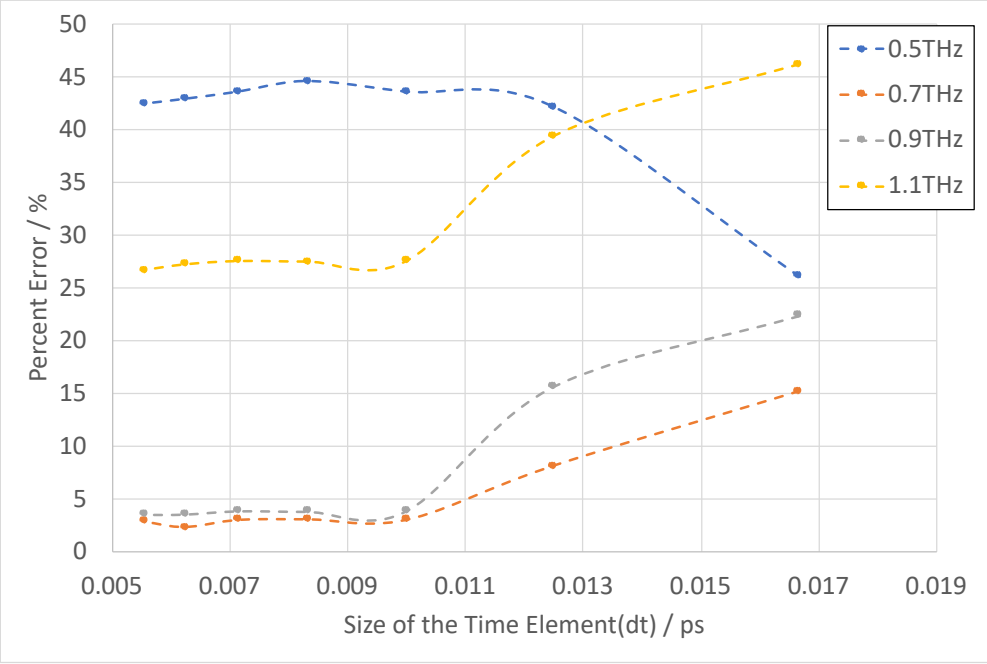

Figure 4.11: Variation of percent error of calculated electron density values with different time resolution for $1x10^{14}$ cm^{-3} electron density.

In Figure 4.10, at low frequencies around 0.5 THz, simulations run with high electron densities show higher percent error. A possible reason for this could be the relationship between electron density and collision frequency. Figure 4.12 shows how the calculated electron density changes when simulations are run with at varying input collision frequencies for 1THz pulse. For this set of simulations, the input electron density value was set to $1x10^{14}$ cm^{-3}. Figure 4.12 indicates very accurate results for a collision frequency of approximately $0.65*10^{12}$ s^{-1}. This corresponds to 0.65% of the numerical value of electron density in cm^{-3}.

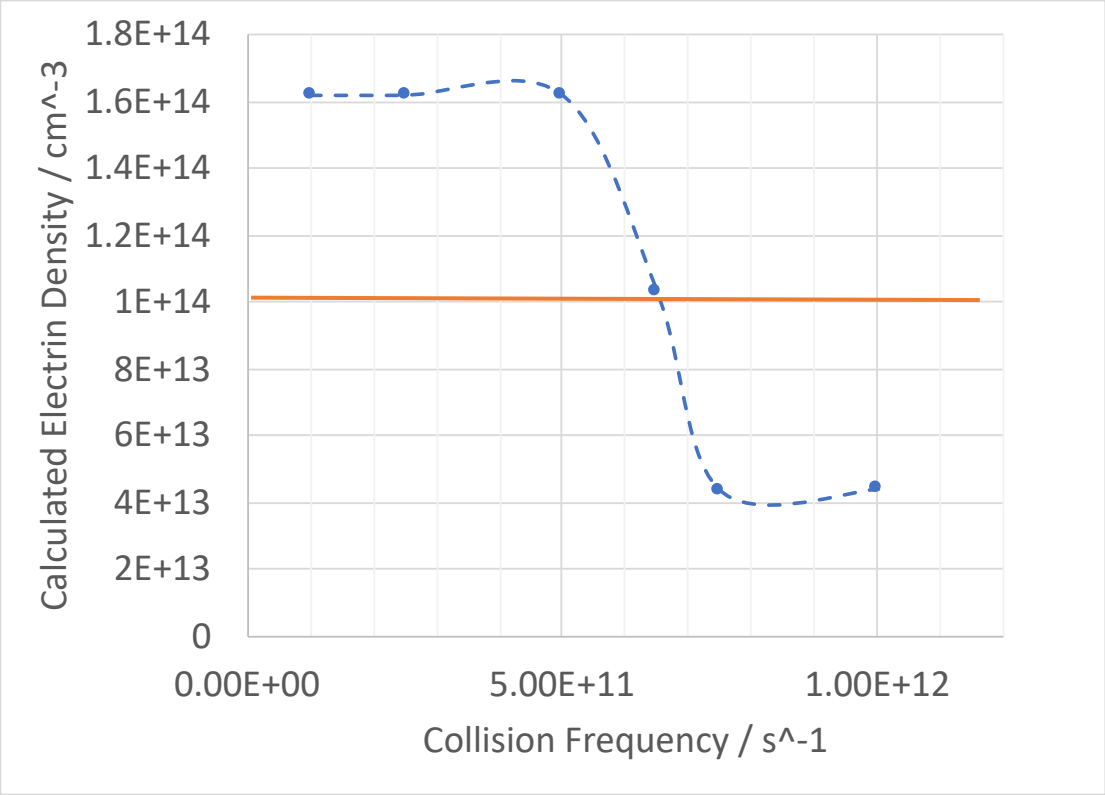

Figure 4.12: Variation of calculated (using 1THz pulse) electron density values (for 1THz pulse) with different collision frequency.

The electron density was then calculated as before but with the assumption that the collision frequency is 0.65% from the numerical value of the electron density in cm^{-3}. This comparison is shown in Figure 4.13. Case 1 corresponds to the collision frequency value set to 1% of the value of electron density in cm^{-3}. Case 2 is when the collision frequency value was inputted 0.65% of the value of electron density in cm^{-3}.

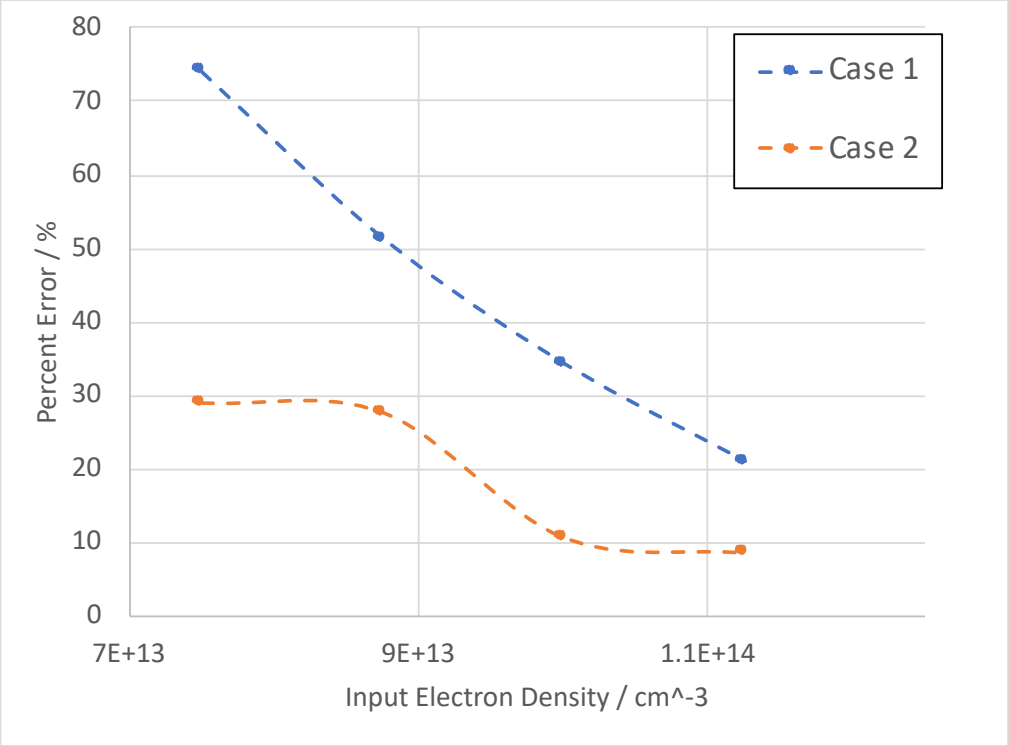

Figure 4.13: Variation of percent error of calculated electron density values for 1THz

radiation with different actual electron densities for Case 1 and Case 2.

Figure 4.13 shows that that the percent error in Case 2 is noticeably less than that for Case 1. This suggests that the Case 2 assumption is better than the Case 1 assumption, but it does not show any linear relationship. The assumption that the relationship between the electron density and collision frequency is linear might not be valid.

4.5 Calculation of refractive index of plasma.

As explained in Chapter 1, phase shift data and Equation 1.21 can be used to calculate the refractive index of the plasma. Those calculated values are shown in Fig. 4.14.

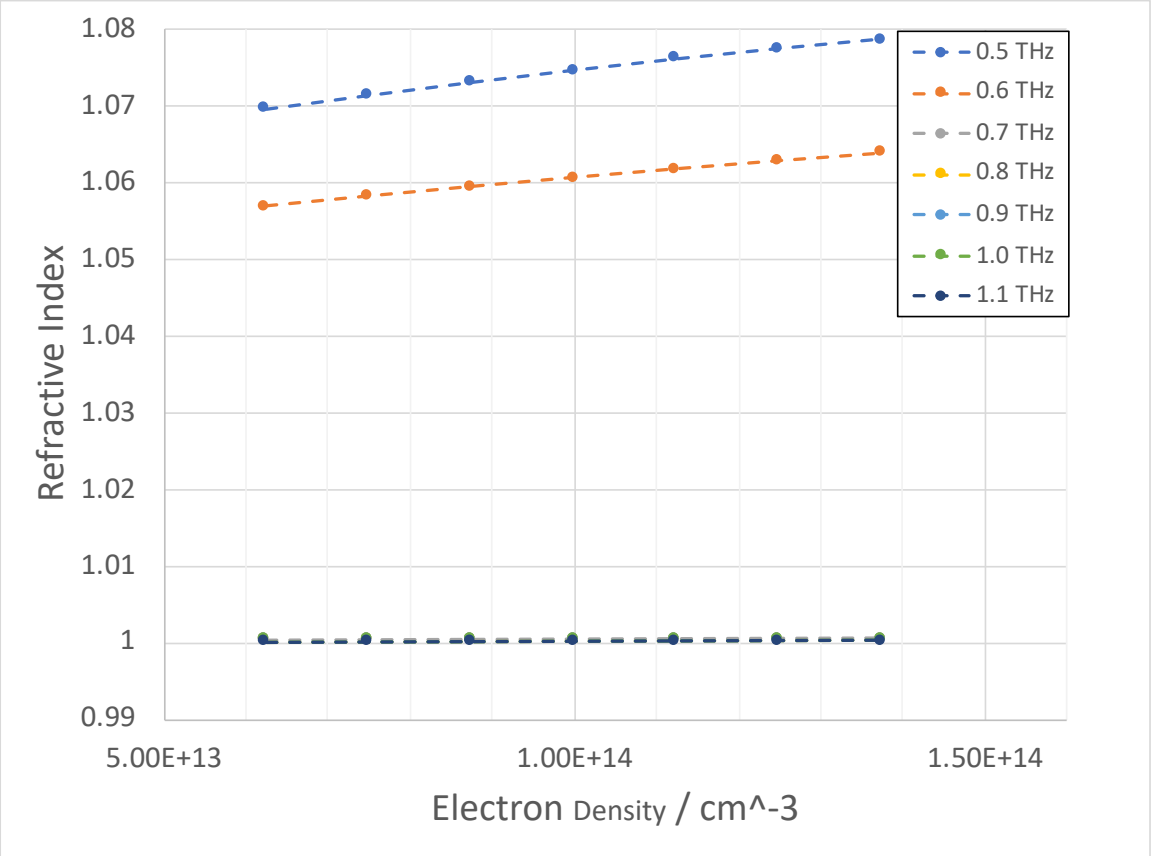

Figure 4.14: Variation of refractive index with electron density and frequency.

The results in Figure 4.14 shows very small changes in refractive index with frequency and electron density. Except for very low frequencies (0.5 THz and 0.6 THz), for all of other frequencies shows refractive index almost equal to 1. It proves that for high frequencies (above 0.7 THz), the plasma medium behaves as if was free space.

5. CONCLUSIONS AND FUTURE WORK

In summary, this thesis work accomplished the preliminar development of a computational model to characterize terahertz light propagation through an unmagnetized plasma. The Finite Difference Time Domain methodology was applied in order to simulate the simple propagation of a THz pulse through a defined medium. The simulation of the complex permittivity of the plasma was accomplished using the Z-transform technique. This yielded the ability to incorporate different plasma properties including the electron density, collision frequency, and interaction length of the plasma medium. From the literature review, the collisional frequency (collision damping term) value was initially taken as 1% of the numerical value of the electron density in cm^{-3} as an assumption. The model provided FDTD simulation results of the propagation of a THz pulse through a plasma as a function of interaction length, electron density, plasma frequency, and collisional frequency.

Data from the FDTD simulations was analyzed using conventional techniques employed in experimental terahertz time-domain spectroscopy. Conversion of the simulated time-domain results into the frequency-domain allowed for characterization of the material parameters. This enabled a calculation from the simulation data of the values of the electron density and refractive index. First, the effects of thickness of plasma and electron density on the intensity of the transmitted terahertz waves were

studied. The results showed that the attenuation of terahertz radiation at a specified frequency of 0.5 THz increased with increasing electron density. Frequencies near the plasma frequency show high attenuation while higher frequencies as compared to the plasma frequency show lower attenuation as expected. The transmittance and absorbance were calculated for as a function of terahertz frequency and varying electron densities. Results indicate that the transmittance increases with frequency and absorbance decreases with frequency. Similarly, when the electron density increases, transmittance decreases, and absorbance increases as the plasma frequency increases with electron density. Transmittance and absorbance variations with frequency and electron density show similar behavior as found in the literature.

The electron density values were calculated from the modeled terahertz time-domain spectroscopy experiment by analysis of the accumulated phase shift and compared with the values that were input originally into the simulation model. The results show multiple different features. One is the calculated electron density values show high deviation from the actual value for high frequencies. The time resolution was investigated as a possible source of this discrepancy. Increasing the time resolution yielded more accurate values for the electron densities.

Changing the relationship between electron density and collision frequency provided more accurate results. This indicates that the assumed relationship between electron density and collision frequency (1% of numerical value of the electron density in cm^{-3}) may not be a very accurate assumption.

Finally, the refractive index was calculated using the phase change of the terahertz wave. The results do not show much variation of the refractive index but the refractive index slightly increase with the electron density.

5.2 Future works.

Considerable future study with this model is now anticipated to improve the accuracy of results. First, one area for improvement is to increase the time resolution to produce more accurate and robust results. A better understood relationship between electron density and collision frequency is required in order to improve the model. In addition, the calculated refractive index values should be validated with experimental measurements. This method can be modified to simulate non-homogenous electron density distributions and magnetized plasma mediums. Finally, the simulation codes should be expanded to incorporate a fully three-dimensional model.

REFERENCES

[1]. K. Wiesemann, “A Short Introduction to Plasma Physics”, CERN Yellow Report CERN-2013-007, pp.85-122, 2013.

[2]. P. Gibbon, “Introduction to Plasma Physics”, CERN, 2016.

[3]. B. H. Kolner, R. A. Buckles, P. M. Conklin, and R. P. Scott, “Plasma Characterization with Terahertz Pulses”, ieee journal of selected topics in quantum electronics, vol. 14, no. 2, march/april 2008.

[4]. J. Neua and C. A. Schmuttenmaer,” Tutorial: An introduction to terahertz time domain spectroscopy (THz-TDS)”, J. Appl. Phys. 124, 231101,2018.

[5]. N. Khiabani, “Introduction to the Terahertz Band”, technical article in All About Circuits, 2019.

[6]. L. Duvillaret, F. Garet, J. F. Roux, and J. L. Coutaz, “Analytical Modeling and Optimization of Terahertz Time-Domain Spectroscopy Experiments Using Photoswitches as Antennas”, ieee journal on selected topics in quantum electronics, vol. 7, no. 4, july/august 2001.

[7]. H. Murakami, K. Serita, Y. Maekawa, S. Fujiwara, E. Matsuda, S. Kim, I. Kawayama and M. Tonouchi,” Scanning laser THz imaging system”, J. Phys. D: Appl. Phys. 47, 2014.

[8]. E. P. J. Parrott, Y. Sun, E. P. MacPherson, “Terahertz spectroscopy: Its future role in medical diagnoses”, Journal of Molecular Structure 1006 (2011) 66–76, 2011.

[9]. M. Naftaly and R. E. Miles, “Terahertz Time-Domain Spectroscopy for Material Characterization”, IEEE, Vol. 95, No. 8, August 2007.

[10]. D. Jang, H. S. Uhm, D. Jang, M. S. Hur, and H. Suk, “Electron density characterization of inductively-coupled argon plasmas by the terahertz time-domain spectroscopy”, Plasma Sources Sci. Technol. 25 (2016) 065008, 2016.

[11]. N. P. Brown, A. M. Steinberg, J. A. Deibel and M. L. R. Walker, “ Assessment of the Capability of Terahertz Time-Domain Spectroscopy as a Plasma Diagnostic”, AIAA Propulsion and Energy Forum, 2020.

[12]. A. Ando, T. Kurose, V. Reymond, K. Kitano, H. Kitahara, K. Takano, M. Tani, M. Hangyo, and S. Hamaguchi, “Electron density measurement of inductively coupled plasmas by terahertz time domain spectroscopy (THz-TDS)”, Journal of Applied Physics 110, 073303, 2011.

[13]. S. P. Jamison, Jingling Shen, D. R. Jones, R. C. Issac, B. Ersfeld, D. Clark, and D. A. Jaroszynski, “Plasma characterization with terahertz time–domain measurements”, Journal of Applied Physics 93, 4334, 2003.

[14]. A. taflove, and S. C. Hagness,” finite-difference time-domain solution of maxwell’s equations”, Wiley Encyclopedia of Electrical and Electronics Engineering, 2016.

[15]. W. Maoyan, Z. Meng, L. Guiping, J. Baojun, Z. Xiaochuan, X. Jun,” FDTD Simulation on Terahertz Waves Propagation Through a Dusty Plasma”, Plasma Science and Technology, Vol.18, No.8, Aug. 2016.

[16]. Y. Baba and V. A. Rakov, “Electromagnetic Computation Methods for Lightning Surge Protection Studies”, vol 3, 2016.

[17]. K. S. Yee,” Numerical Solution of Initial Boundary Value Problems Involving Maxwell’s Equations in Isotropic Media”, IEEE Trans. Antennas Propag. 14,pp 302–307, 1966.

[18]. EMPossibel, “Formulation of One-Dimensional FDTD” 2020.

[19]. A. Taflove, “Computational electrodynamics: The finite different time domain method. 1995.

[20]. A. Z. Elsherbeni, V. Demir, “The Finite-Difference Time-Domain Method for Electromagnetics with MATLAB Simulations” 2nd Edition, 2015.

[21]. D. M. Sullivan, “Electromagnetic Simulation using the FDTD method”, Second Edition, 2013.

[22]. K. R. Umashankar, “Finite-Difference Time Domain Method”,Ch 06,

[23]. D. M. Sullivan, “Exceeding the Courant Condition with the FDTD Method”, ieee microwave and guided wave letters, vol. 6, no. 8, august 1996

[24]. D. M. Sullivan, “Z transform theory and the FDTD model, ieee transactions on antennas and propagation, vol. 44, no. 1, january 1996.

[25]. P. Ciampolini, P. Mezzanotte, “Accurate and Efficient Circuit Simulation with Lumped-Element FDTD Technique”, ieee transactions on microwave theory and techniques, vol. 44, no. 12, december 1996.

[26]. P. J. Ford, S. R. Beeson, H. G. Krompholz, and A. A. Neuber," A finite-difference time-domain simulation of high-power microwave generated plasma at atmospheric pressures", Physics of Plasmas, 19, 073503. 2012

[27]. D. N. Smithe, "Finite-difference time-domain simulation of fusion plasmas at radiofrequency time scale", Physics of Plasmas 14, 056104 .2007.

[28]. M. Liu, X. Hu, Z. Jiang, S. Zhang, and C. Lan," Attenuation of wave in a thin plasma layer by finite-difference time-domain analysis", Journal of Applied Physics 101, 053308 2007.

[29]. B. H. Kolner, P. M. Conklin, N. K. Fontaine, R. A. Buckles, and R. P. Scott," Terahertz characterization of pulsed plasmas", Optical Society of America, 2005.

[30]. K. Kang, D. Jang and H. Suk," Plasma density measurements using THz pulses from laser-plasmas", 18th International Symposium on Laser-Aided Plasma Diagnostics, 24–28 September 2017.

[31]. N. P. Brown and A. M. Steinberg, "Assessment of the Capability of Terahertz Time-Domain Spectroscopy as a Plasma Diagnostic", American Institute of Aeronautics and Astronautics, 2020.

[32]. P. P. Pawar ," Measurement of mass and linear attenuation coefficients of gammarays of Al for 514, 662 and 1280 keV photons", J. Chem. Pharm. Res., 2011, 3(4): 899-903

APPENDIX I

MATLAB code for FDTD simulation of plasma medium.

```
%%%%1D FDTD simulation through plasma medium%%%
clear all

%Simulation Parameters.
KE=8000; % Length of the space.

ddx=1e-5;    %Define the Yee cell dimension.
dt=ddx/6e8;  %Define the size of the time element.

kstart=200; %Start point of plasma medium.
kend=1200; %End point of plasma medium.

nsteps=5000; % Number of time steps.

% Define ex, dx and sx empty arrays.
ex=zeros(1,KE);
dx=zeros(1,KE);
hy=zeros(1,KE);
ix=zeros(1,KE);
sx=zeros(1,KE);
sx1=zeros(1,KE);
sx2=zeros(1,KE);

t0=150.0; % Starting time of the pulse.
spread=15; % Spread of the pulse.

% Starting an absorbing Boundary Conditions.
ex_low_m1=0.0;
ex_low_m2=0.0;
ex_high_m1=0.0;
ex_high_m2=0.0;


%%%MAIN FDTD LOOP%%%

T=0;
for n=1:nsteps
    T=T+1;

    %Updating electric field in free space.
    for k=2:KE
        dx(k)=dx(k)+(0.5)*(hy(k-1)-hy(k));
    end
```

```
% Source Pulse
    pulse=-1*((t0-T)./spread).*exp(-0.2.*((t0-T)./spread)^2);

    dx(5)=dx(5)+pulse;

    for k=2:KE

    %Incorporate the plasma medium.
        if (k >= kstart && k <= kend)
            ne=1e20; %Electron density.
            e=1.6E-19; %Charge of an electron.
            me=9.11E-31; %Mass of an electrum.
            omega=((ne*e^2)/(me*epsz))^(1/2);% Calculate the plasma
frequency.

            vc=ne*0.65/1E8;%Relationship between electron density and
collision frequency.

            %Updating electric field inside the plasma medium.
            ex(k)=(dx(k)-sx1(k));
            sx(k)=(1+exp(-vc.*dt)).*sx1(k)-exp(-
vc.*dt).*sx2(k)+((omega^2).*dt/vc).*(1-exp(-vc.*dt)).*ex(k);
            sx2(k)=sx1(k);
            sx1(k)=sx(k);

     else
           ex(k)=dx(k);
       end

    end

    % Absorbing Boundary Conditions.
        ex(1)=ex_low_m2;
        ex_low_m2=ex_low_m1;
        ex_low_m1=ex(2);

        ex(KE)=ex_high_m2;
        ex_high_m2=ex_high_m1;
        ex_high_m1=ex(KE-1);

    % Updating magnetic field
        for k=1:KE-1
            hy(k)=hy(k)+(0.5)*(ex(k)-ex(k+1));
        end

    %Plot the electric field component with time.
        plot(ex,'b','LineWidth',1.5)
        rectangle('Position',[kstart, -1.5,kend-kstart,
3],'LineWidth',1.5)% Plasma medium.
        grid on
        text((401),1.4,' Plsama Material');
        text((101),1.4,'   Free Space');
        text((1401),1.4,'   Free Space');
        title(['Time = ',num2str(n)]);
        pause(0.002)
end
```

MATLAB code for Terahertz Time Domain Analysis

```
clc
clear
clf
format long

%input data from the reference signal
data1=uigetfile('*.txt','Select the file containing the reference
signal');
datum1=dlmread(data1,'\t');
signal1=datum1(:,2);

%compute the time per step in ps
delta= datum1(2,1)-datum1(1,1);

%calculate the number of data points
n=size(datum1,1);

%create a time array
for q=1:1:n
    timeindex(q,1)=(q);
    timeps(q,1)=(q-1)*delta;
end
time=timeps.*1e-12;


plot(timeps,signal1,'r-')
    xlabel('Time');
%     xlim([0, 3e-12])
    ylabel('Terahertz Signal (a.u.)')
    title('THz Signal Propagation through air(red) and Sample(blue)')


[x,y]=size(signal1);

realtime=time;
realtimeps=realtime.*1e12;

signal1a=signal1;
%signal2a=signal2;

disp('You now need to enter the number of samples for the FFT
procedures')
disp('Enter 10 for 1024 samples')
disp('Enter 11 for 2048 samples')
disp('Enter 12 for 4096 samples')
disp('Enter 13 for 8192 samples')
disp('Enter 14 for 16384 samples')

samples=input(' ');

%number of samples
nfft=2^samples;
fsample=x/((time(x,1)-time(1,1)));
```

```
fn=(nfft/2:nfft)';
freqaxis=(fsample*(fn-nfft/2)/nfft);
freq=freqaxis*1e-12;

%fft of the signal transmitted through air
J1=fft(signal1a,nfft);
J1=fftshift(J1);
J1a=J1(fn);
J1b=abs(J1a);

%normalize reference plot
J1c=sort(real(J1b));
signalmax1=J1c(nfft/2,1);
J1norm=(real(J1b))./signalmax1;

max=input('Please enter the maximum freq you wish displayed on the
Frequency Domain Plot\n');

%plot the fft of the sample signal
%plot(freq,real(J1b),'r')
semilogy(freq,real(J1b),'r')
    axis([0,max,0,signalmax1])
    xlabel('Frequency (THz)')
    xlim([0 5e12])
    ylim([1e-2 1e2])
    ylabel('Power Spectrum')
    title('THz Signal Propagation through Air(red), Sample (blue) ')
   disp('Please press any key to continue')
   pause

grid off

disp('Please press any key to continue')
pause

signalphase1=unwrap(angle(J1a));

plot(freq,signalphase1,'r')
xlabel('Frequency (THz)')
xlim([0, 5e12])
ylabel('Signal Phase')
title('Signal Phase Vs Frequency')
disp('Please press any key to continue')
pause

grid off
```